



HAL
open science

Focal Point: Imaging Optical Near-field in Plasmonic Nanostructures

Alexandre Merlen, François Lagugné-Labarthet

► **To cite this version:**

Alexandre Merlen, François Lagugné-Labarthet. Focal Point: Imaging Optical Near-field in Plasmonic Nanostructures. *Applied Spectroscopy*, 2014, 68, pp.1307-1326. 10.1366/14-07699 . hal-01191524

HAL Id: hal-01191524

<https://hal.science/hal-01191524>

Submitted on 2 Sep 2015

HAL is a multi-disciplinary open access archive for the deposit and dissemination of scientific research documents, whether they are published or not. The documents may come from teaching and research institutions in France or abroad, or from public or private research centers.

L'archive ouverte pluridisciplinaire **HAL**, est destinée au dépôt et à la diffusion de documents scientifiques de niveau recherche, publiés ou non, émanant des établissements d'enseignement et de recherche français ou étrangers, des laboratoires publics ou privés.

Focal Point: Imaging Optical Near-field in Plasmonic Nanostructures.

Alexandre Merlen¹ and François Lagugné-Labarthe²

¹ Institut Matériaux Microélectronique Nanosciences de Provence (IM2NP) UMR CNRS 7334 & Universités d'Aix-Marseille et de Toulon, France.

² Western University (The University of Western Ontario), Chemistry Department and Centre for Materials and Biomaterials, 1151 Richmond street, London, On, N6A5B7, Canada

Corresponding authors: merlen@univ-tln.fr and flagugne@uwo.ca

Over the past five years, new developments in the field of plasmonics have emerged with the desire to finely tune a variety of metallic nanostructures to enable a desired function. The use of plasmonics in spectroscopy is of course of great interest due to large local enhancements in the optical near-field confined in the vicinity of a metal nanostructure. For a given metal, such enhancements are dependent on the shape of the structure as well as the optical parameters (wavelength, phase, polarization) of the impinging light, offering a large degree of control over the optical and spatial localization of the plasmon resonance. In this focal point, we highlight recent work that aims at revealing the spatial position of the localized plasmon resonances using a variety of optical and non-optical methods.

INTRODUCTION

Metallic nanostructures have enabled critical advances in a variety of applications ranging from metatronics devices to perform a specific logical function,¹ medical research to better target tumors for further localized photothermal treatment,^{2, 3} surface-driven catalytical reactions,⁴ solar cells technology^{5, 6} to high sensitivity optical sensors and spectroscopic analysis of biochemicals and chemicals.⁷⁻¹⁰ The electromagnetic field confined in the vicinity of a single metallic nanoparticle or an ensemble of interacting particles, displays resonances and localizations that are dependent not only on the considered metal but also on the opto-geometric properties of the nanostructure. The control of localized surface plasmon (LSPR) resulting from the interaction between an electromagnetic field and a metallic surface is therefore critical for the development of applications that yet have to be explored.¹¹ The specific use of

engineered plasmonic platforms or plasmonic tips in the field of Raman spectroscopy is noteworthy and a re-birth of surface-enhanced spectroscopy 40 years after its discovery has led to a variety of applications ranging from pollutant monitoring,¹² molecular recognition in microfluidics devices,¹³ cell biology,¹⁴ ultrasensitive measurements in the biomedical field,¹⁵ to high spatial resolution vibrational spectroscopy benefiting from tip-enhanced effect.¹⁶⁻¹⁸

To tailor LSPR for a particular application, the design and the fabrication method are ultimately the two factors that critically define the response of the structure to the impinging field.¹⁹ For example, gold nanostructures with submicron sizes will have resonances in the visible spectrum opening applications in surface-enhanced Raman spectroscopy (SERS)²⁰⁻²² while structures with the same geometry but with dimensions of several microns will have resonances in the mid-infrared spectral range opening surface enhanced infrared spectroscopy applications (SEIRS).^{23, 24} The use of plasmonic platforms in surface enhanced fluorescence (SEF) are also promising yielding higher spatial resolution, shorter acquisition time or smaller irradiance.²⁵ For general surface enhanced spectroscopy, the spectral matching between the input wavelength and the LSPR is not very critical since the spectral width of the LSPR is generally large enough so that resonances and subsequent enhancements are effective even if resonance conditions are not perfectly met. However, for other applications where a perfect matching and a high degree of confinement are necessary, such as in high resolution imaging, the experimental spectral and spatial characterization of the LSPR is of particular interest.

In the present focal point, we report on recent work where various techniques are used to map localized surface plasmon in the vicinity of metallic nanostructures. Several reviews have already been written on this topic,²⁶⁻²⁹ yet recent progress in the field has been evolving rapidly as well as the multiple approaches to manipulate surface plasmon. Optical measurements are naturally primarily used in various combinations using near-field scanning methods or far-field microscopies to probe a variety of linear or nonlinear optical processes.

From a pure spectroscopy aspect, if a majority of recently published work focuses on plasmon mediated SERS, recent work on nonlinear optical applications of plasmonic structures are making use of resonances with incoming short pulse of light highlighting new potentials in nanophotonics.³⁰ Of great interest, advanced electronic microscopy methods with electronic excitation and/or electron emission methods are reviewed and show clearly the localization of resonance for given energies with unprecedented spatial resolution. Last, indirect methods involving surface deformation of a photosensitive material, or thermal effects are also described. The use of an atomic force microscope probe to sense weak local forces (down to 10^{-15} Newton) from the confined optical field is also an elegant approach evidenced by recently published work.

OPTICAL NEAR-FIELD MICROSCOPY

Since plasmonic nanostructures are commonly used for optical applications, it appears logical to use optical techniques for the study of their near-field properties. Nevertheless, the spatial resolution of optical microscopy measurements is diffraction limited and the expected spatial resolution is typically half of the effective optical wavelength as described by Abbe's criterion. This resolution, typically a few hundred nanometers, is much larger than the typical size of the evanescent field confined in the vicinity of metallic nanostructures, which is limited to a few nanometers. It is therefore necessary to surpass this diffraction limit to reach a better spatial resolution of the optical measurement. In this context, optical near-field microscopy is a technique of choice and is based on an optical probe with a dimension much lower than the wavelength that is used to convert the non-propagative optical near-field signal into a measurable far-field contribution. Using a scanning near-field optical microscope (SNOM) it is thus possible to map the optical properties of plasmonic nanoparticles with a spatial resolution in the ~ 10 nm range. SNOM can be conducted on a variety of samples with distinct optical schemes such as collection or illumination modes. The near-field mapping can be performed with a large choice of excitation sources limited only by the current laser tunability range. As a consequence, SNOM experiments on plasmonic structures are often performed by changing the geometrical parameters of the nanostructure rather than changing the photon energy. A comprehensive description of near-field optical microscopy and the interpretation of the collected images can be found elsewhere.³¹⁻³³

The critical factor in SNOM relies on the optical probe: its dimension must be small enough to obtain a high spatial resolution and it must be extremely efficient for the conversion of the optical near-field into a measurable far-field signal. In addition, the probe must be localized in the near-field of the sample, typically a few nanometers from the surface in order to convert the evanescent waves into propagative waves. A critical issue is the role of the probe that perturbs the optical near-field, yielding images that can be complex to analyze.³⁴⁻³⁶ In addition, the mechanical interaction between the probe and the sample can also induce artifacts in the image that must be carefully considered.³⁷ Based on the nature of the probe, SNOM techniques can be classified in the "aperture" and "apertureless" categories as depicted in Fig.1(A). Herein we describe both techniques and elaborate on how they can be used to map the near-field of metallic nanostructures.

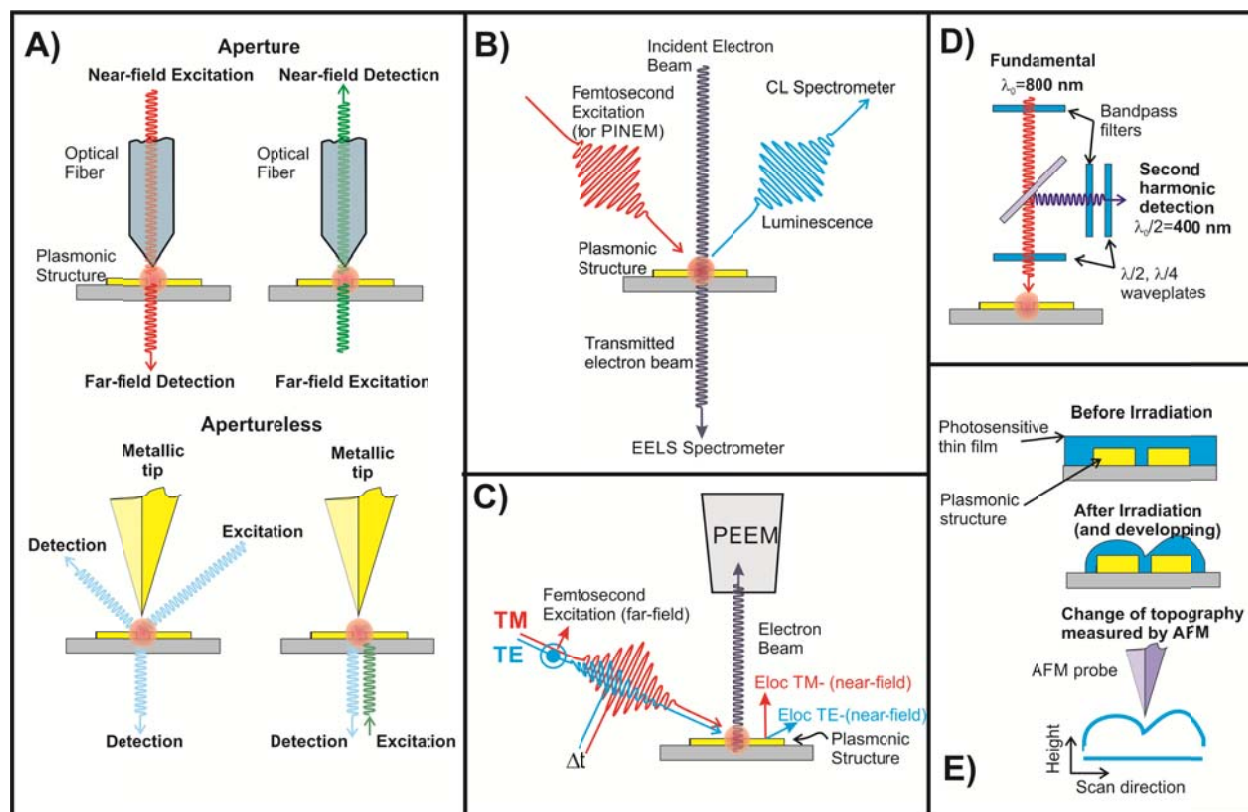


Fig.1. (A) Scanning near field microscopies using optical fiber probe (“with aperture”) or metallic tips (“apertureless”). (B) Electronic microscopies. Cathodoluminescence is performed using electronic excitation and optical collection and analysis of the collected luminescence. EELS uses both electronic excitation and collection. (C) Photoemission electron microscopy (PEEM). A laser source such as a femtosecond laser induce electron emission detected by the electron microscope. Pulse duration, polarization, phase and angle of incidence of the input beam can be tuned to excite the nanostructure. (D) Second harmonic generation (SHG) microscopy of plasmonic structure involves a fundamental excitation source with frequency ω that can be tunable. To avoid damage in metallic structures, femtosecond pulses with high repetition rate (80 MHz range) are generally used. The detection is performed at 2ω . A series of optical bandpass filters must be used to discriminate SHG from two-photon induced luminescence effects from the metallic nanostructure. (E) Indirect methods based on the use of a photosensitive thin film coated over the plasmonic structure. Upon irradiation with an irradiance set at the threshold value, the photosensitive thin film undergoes physical changes that can be probed by AFM or SEM. The local changes indicate the location of the hot spots.

Aperture SNOM (a-SNOM). With a-SNOM the probe is generally an optical fiber with a nano-aperture at the apex (Fig.1(A)).³⁸ The tip is metalized (Aluminum usually) and only the apex of the tip is opened to provide a better confinement of the electromagnetic field. Alternatively, cantilevered hollow silicon atomic force microscope (AFM) probes with nanoaperture can also be used to perform near-field optical measurements.³⁹ The typical control of probe-sample interaction is based on shear forces measured with a tuning fork or with a standard AFM controller.⁴⁰ If the optical excitation (respectively the

detection) is passing through the aperture, the excitation (or detection) is qualified of “near-field” while the detection (respectively the excitation) is performed in the “far-field”. Different configurations of near and far-field excitation and detection can be performed. For the study of plasmonic nanostructures, a variety of optical signals can be measured using SNOM (Fluorescence, Luminescence, elastically or inelastically light scattered, second or third harmonic generation,...). In most of SNOM studies, the elastically scattered light is generally measured as well as other advanced measurements such as fluorescence,⁴¹ two-photon induced luminescence (using near infrared and ultrashort laser pulses)⁴²⁻⁴⁴ or second harmonic generation.^{18, 39, 45} Each technique can bring specific information about the studied sample and the combined use of different measurements for a complete analysis of both the scattering response and local field distribution has already been pointed out.⁴⁶ In addition aperture SNOM offer the possibility to perform near-field polarimetric measurements.⁴⁷ The main issue of a-SNOM setups is the limited collection or detection efficiency. Also, large input power of the excitation light can cause irreversible thermal damages to the tip. In addition if we assume that transmission in a metallic aperture is proportional to a^4 (with a being the diameter of the aperture) a decrease of this size by an order of magnitude will decrease the signal intensity by 10^4 . As a consequence, a-SNOM is limited to very efficient optical processes that can be collected using reasonable acquisition time to avoid possible mechanical drift of the positioning stage. Often, a compromise must be found between resolution, requiring a small aperture diameter, and signal intensity. In most a-SNOM studies the typical diameter of the aperture is around 50 nm. Typical near-field images of metallic nanostructures obtained with a-SNOM can be seen in Fig. 2(A,B).^{48, 49} A good agreement between the experimental near-field measurement and the modeling of the optical near-field is shown in Fig. 2(A) as long as the limited resolution of SNOM measurements is taken into account. Experimental developments have highlighted that a-SNOM can be combined with femtosecond laser excitation to visualize the ultrafast response of plasmonic nanostructures.⁵⁰ A-SNOM has a rather limited spatial resolution (typically a few 10 nanometers in the ideal conditions) and is not well suited for the study of nanostructures with smaller dimensions. To improve this resolution, photon scanning tunneling microscope (PSTM, or Scanning Tunneling Optical Microscope STOM) has been developed. Bottom illumination induces total internal reflection in the sample. The evanescent field at the surface is converted in a far-field signal by a dielectric nano-aperture. Since there is no metallic coating at the surface of the probe, the confinement of the electromagnetic fields at the apex is higher and the expected resolution is better.⁵¹ This technique has been used for the study of plasmonic nanostructures.^{52, 53} It must be noticed that aperture SNOM can also be used to measure near-field magnetic properties of plasmonic nanostructures.⁵⁴

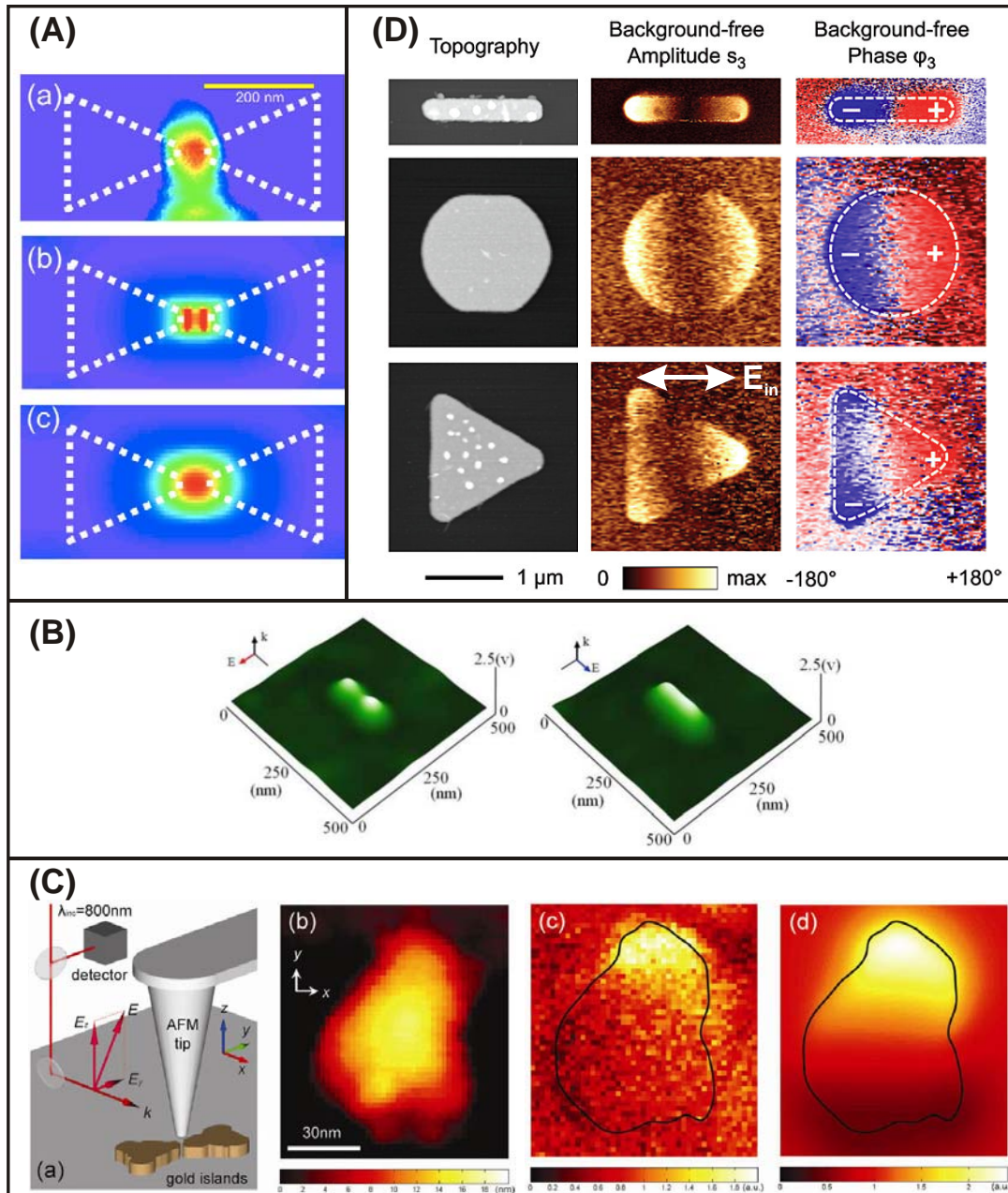


Fig. 2. (A) (a) UV (364 nm) aperture near-field images of an aluminum bowtie nanoantenna. The “hot-spot” in the gap is clearly visible. (b) and (c) are corresponding FDTD simulations. The calculated image (c) takes into account the limited resolution of a-SNOM. (Adapted with permission from ref. 48) (B) Aperture near-field mapping of a gold nanoparticles (diameter=50 nm) pair. The image is recorded for two perpendicular laser (532 nm) polarizations. (Adapted with permission from ref. 49) (C) (a) Schematic of a s-SNOM experiment. The tip is made of silicon and second harmonic demodulation is used. The topography (b), near-field image (c) and simulation (d) of a gold nanostructure are reported. (Reprinted with permission from ref. 56, Copyright 2012, AIP Publishing LLC) (D) Topography (left) and apertureless IR ($9.6 \mu\text{m}$) near-field images of a metallic triangle. The optical image is obtained using interferometric detection, dielectric tips, higher harmonic demodulation and residual background subtraction. With this configuration both amplitude and phase images can be acquired. (Adapted from ref. 60 with permission of American Chemical Society, Copyright 2010)

Apertureless SNOM (s-SNOM). In many examples, the spatial resolution of aperture SNOM is not sufficient to probe accurately the optical near-field confined in the vicinity of plasmonic nanostructures. As an alternative, s-SNOM has been proposed.⁵⁵ As shown in Fig. 1(A), the optical probe is a metallic or metallized tip playing the role of a nanoantenna to convert the near-field information into a far-field and measurable signal.⁵⁶ Some studies have proven that in such a configuration, the spatial resolution can be very high and suitable for the study of plasmonic nanostructures.^{57, 58} Different configurations of optical excitation and collection have been developed offering a variety of control over the input/output polarization, the incidence angle, the optical collection and finally the transparency of the sample or substrate. Usually two main configurations are used: side-illumination and/or collection and bottom-illumination and/or collection. For side-illumination the optical collection is usually weak for technical reasons. It is much higher with bottom illumination but it requires a transparent substrate. Other optical configurations have also been proposed for specific measurements.⁵⁹ It must be noticed that s-SNOM can be performed in a wide range of excitation wavelengths including the infrared spectral region.⁶⁰ Some typical images of plasmonic nanostructures obtained with this technique are reported in Figs. 2(C) and 2(D).^{56, 60} The efficiency of the tip and the reproducibility of its fabrication are both critical parameters for s-SNOM measurements. Advanced nanofabrication methods are aiming at producing photonic-plasmonic tips designed for specific applications such as Raman SERS measurements providing high sensitivity as well as high spatial resolution.⁶¹ In most cases the nature of the optical interaction between the tip and the sample is not clearly understood and it is absolutely necessary to be extremely cautious in the analysis of the obtained images. In this context, numerical modeling such as finite difference time domain (FDTD) and discrete dipole approximation (DDA) are valuable tools for a fine interpretation of the images. Different kind of tips can be used for s-SNOM studies of metallic nanostructures. Fluorescent functionalized tip are used to probe the near-field enhancement through an increase of the fluorescence induced by the plasmonic structure. In such experiments, the distance between the fluorescent tip and the metal surface must be well controlled to prevent quenching effects.⁶²⁻⁶⁵ A mapping of the sample with the tip finally gives the distribution of optical hot-spots. However the spatial resolution obtained with such functionalized tip is usually less than non-functionalized AFM tips. To improve the resolution of s-SNOM, metallic tips made of gold or silver were used to interact with the near-field of plasmonic nanostructures. Elastically scattered light due to tip-sample interaction is measured and improvement of the resolution can be done by inscribing a grating on the tip to optimize the coupling of the input light with the nanoantenna.⁶⁶ A major issue with such metallic tip is the presence of a strongly enhanced electromagnetic field at its apex. The interaction between the tip-enhanced field and the field from the plasmonic nanostructures can be rather complex as shown by numerical simulations and the final mapping is a snapshot

of this interaction. As possible alternatives the use of semi-conducting tips such as silicon,⁶⁷ nanotubes,⁶⁸ and carbon⁵⁹ has been proposed to reduce tip-sample interaction.

In any case, the collected signal is often noisy with a strong background signal coming from all the collected light not related to the field scattered by the tip. To improve this major drawback two different approaches have been proposed. The first one is based on an oscillating tip (Non-contact or tapping AFM modes) combined with a lock-in detection: only scattered light modulated at higher harmonics of the tip frequency oscillation is measured, removing the entire background signal. The use of this method in SNOM for the reduction of noise has already been demonstrated.⁶⁹⁻⁷¹ Usually second harmonic⁶⁷ or third harmonic⁷² detection is used. Higher harmonics detection makes the near-field contribution⁷³ sharper at the cost of a weaker signal. In addition, it is absolutely necessary to check that the detected anharmonic signal does not come from pure mechanical artifacts (tip touching the surface in tapping mode, non-harmonic tip surface interaction).⁷⁴

The second method for background suppression is based on the use of an interferometric scheme. It has been shown that in a-SNOM the final image is the result of a subtle combination of various interferometric signals.⁷⁵ Such feature can be used for background suppression: a frequency shifted reference beam is used to make interferences with the tip scattered light. In such heterodyne detection the background signal can be significantly removed using lock-in detection. The advantages of this method compared to non-interferometric has been discussed in several articles.^{76, 77} In addition to field intensity, heterodyne detection enables phase-contrast images which bring a valuable set of informations (Fig.2(D)).⁶⁰ Added to this configuration the use of a cross-polarization side illumination and detection enhance the signal-to-noise ratio.⁷⁸ This last point is the major drawback of SNOM: the exact role of the near-field probe remains unclear. Essingler et al. have recently indicated that the final measured signal is directly proportional to the field of the coupled tip-sample system.³⁴ A post treatment deconvolution is thus required to get only the field from the sample. It is then necessary to know exactly the optical properties of the probe which remains an experimental challenge.

In conclusion, optical near-field microscopy can be very efficient for the study of plasmonic modes in metallic nanostructures. Nevertheless it should be clearly emphasized that the final interpretation of the images strongly depends on the nature of the probe-sample interaction.

ELECTRON MICROSCOPY

Local information on plasmons can be obtained using electrons. Plasmons are associated to collective electronic oscillations and they can easily couple to moving charges giving rise to a detectable interaction. The nature of this interaction depends on the observation mode,⁷⁹ and it has been demonstrated that it can be used to determine the local density of state (LDOS) of plasmons. Electron microscopy is usually used to have information about the morphology, crystallographic and structural properties of nanostructures. In scanning electron microscopy (SEM) the collected images are generated using either secondary or backscattered electrons. The expected resolution is typically a few nanometers due to the capacity to focus the electron beam very tightly. In a transmission microscope (TEM) the electron beam transmitted through the sample is detected and its spatial resolution is much higher than with a SEM. However the main disadvantage is that the sample must be transparent to electrons. It must be extremely thin and the preparation of a sample for TEM can require multiple preparation steps by electron beam milling. In addition, all electronic microscopy techniques require high vacuum and conductive samples. Despite those drawbacks the high spatial resolution of electron microscopy is extremely promising for the study of optical near-field properties of plasmonic nanostructures. Two main approaches have been developed for such measurements: cathodoluminescence (CL) and electron energy loss spectroscopy (EELS) as depicted in Fig. 1(B).²⁷

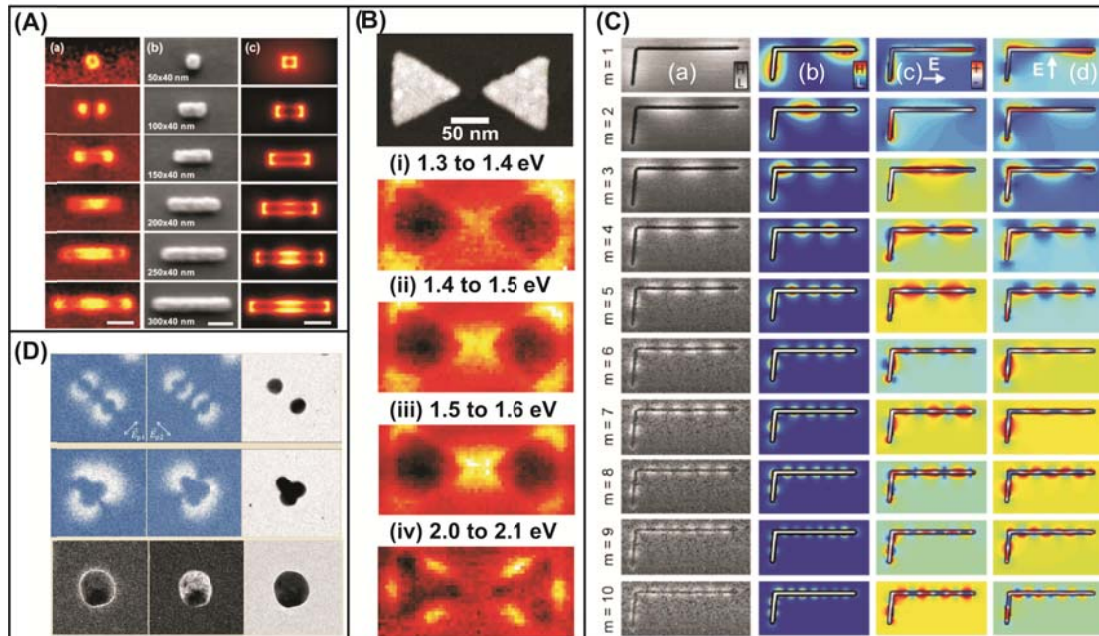


Fig. 3. (A) CL excitability images of various aluminum nanorods for the energy range 2.5-3 eV (left) associated with the electron microscopy image (middle) and the calculated electromagnetic field distribution (FDTD). The scale bars are 100 nm. (Adapted from ref. 81 with permission of American Chemical Society, Copyright 2012) (B) EELS mapping of gold bowtie nanostructures obtained for various energy ranges. The corresponding electron microscopy image is also reported. The scale

bar is 50 nm. (Adapted from ref. 92 with permission of American Chemical Society, Copyright 2011) (C) Comparison between experimental EELS mapping, calculated EELS signal and optical FDTD simulations for two orthogonal polarizations. The measurements and simulation are performed on a silver bent nanowire (length: 1034 nm). (Reprinted with permission from ref. 89, Copyright (2013) by the American Physical Society (D) Above and middle: PINEM images of silver nanoparticles for two polarizations. The particles in the top panel are separated by 70 nm. (Bottom: EELS images of 45 nm radius particles.) (Adapted from ref. 98 with permission of American Chemical Society, Copyright 2012)

Cathodoluminescence. When a sample is illuminated with an electron beam it can emit light. In the case of semiconducting materials, this light is a result of an electron-hole recombination process. For metallic nanostructures the electron beam excite the oscillating plasmons giving rise to a detectable radiation. Thus the wavelength, intensity and polarization of this radiation all depend on the plasmonic properties of the sample. The electron beam is scanned over the whole plasmonic nanostructures and simultaneously the emitted light is detected. Two informations can therefore be recorded: (i) *a spectral information*: at a given point of the structure, the spectral properties of the emitted light are measured. Such spectrum gives information on the spectral positions of plasmonic modes for the observed nanostructures. The spectral resolution of CL is very high and typically of 1 meV in the visible range.⁸⁰ The polarization of emitted light can also be studied using a polarizer placed in front of the optical detector. (ii) *a spatial information*: for a given emission wavelength, the radiation intensity is scanned over the sample. The final map gives a spatial distribution of the near-field properties of the metallic nanostructures. Both measurements can be performed using either a SEM or a TEM microscope. With a SEM the acceleration voltage is typically a few 10 kV while it is significantly higher with a TEM (200-300 kV). Usually, the background CL signal can be quite high and sometimes require a post treatment analysis in the obtained images. It is therefore beneficial to use a substrate with a low CL signal (silicon wafer for example) in the spectral range of interest. To increase the signal intensity from the sample the electron beam is usually focalized with a rather large spot size (typically 5-10 nm) thus decreasing the spatial resolution. An example of CL mapping performed on aluminum nanorod antennas prepared by lithography can be seen in Fig. 3(A).⁸¹ The influence of the aspect ratio is clearly evidenced and is directly associated to the plasmonic properties of such antennas. For the 100 nm rod a strong dipolar mode is observed whereas for the longest nanostructure, quadrupolar modes are clearly visible. The authors estimated their spatial resolution to be better than 20 nm.

As for any electron-plasmons interaction processes the interpretation of the obtained images is not straightforward. Usually optical modelling of the electromagnetic field using various methods (FDTD, boundary element method....) is required to yield a clearcut interpretation of the mapping. However, the agreement between simulation and experimental measurements is sometimes poor.⁸⁰ It has been clearly shown that

electronic microscopy give a different information compared to pure light processes. Dark modes (i.e. plasmonic modes that cannot be observed using pure optical measurements) can be detected using CL.⁸² It is admitted that the final mapping gives the electromagnetic local density of states (EM-LDOS). In addition, electron beam is more capable of exciting out-of-plane modes of the nanostructures.⁸³ This is a real challenge for the detection of hot-spots between interacting plasmonic features. Such hot-spots play a key role in surface enhanced spectroscopies and can be observed between dimers⁸⁴ giving rise to very intense in-plane electric field. With electronic excitation it is hardly possible to detect this field.

The spatial resolution of CL is not as high compared to usual electronic microscopy. As previously mentioned the electron beam is quite large, but this is not the only factor decreasing the resolution: the CL emission can occur even when the electron passes near the material without actually going through it.^{85, 86} It is generally assumed that this resolution is typically around 10-20 nm. The resolution is slightly higher with a TEM than with a SEM, but the complexity of TEM observations added to the use of high acceleration voltage that can damage the plasmonic nanostructures make the advantages of transmission microscopy for CL measurements not trivial.

Electron energy loss spectroscopy (EELS). EELS is based on a pure electronic mechanism and it can be performed only with a transmission microscope. The EELS signal is related to the energy lost by an electron through its interaction with a given sample. For metallic nanostructures it has been shown that this energy loss is related to the excitation of plasmonic modes. Similar to CL, EELS provides spectral and spatial informations of the plasmonic modes. For spectral analysis, EELS is not so efficient compared to CL for two reasons. On one hand, it is limited to rather high energy modes (typically higher than 1.5 eV which correspond to wavelengths lower than 830 nm) because of the very intense beam (usually called the zero-loss or Rayleigh beam) of the elastically transmitted electron beam. This point can be improved using energy filtering TEM (EF-TEM).⁸⁷ Technical developments are moving forward and some recent studies have reported measurements down to much lower energy, typically 0.5 eV (2500 nm).⁸⁸ On the other hand, the intrinsic spectral resolution of EELS is lower compared to CL: even with a monochromatic source it is difficult to have a resolution better than 100 meV,⁸⁹ this value can be compared to the 1 meV resolution expected with CL measurements. In addition such a high resolution is reached by the cost of decreasing signal intensity. The mapping can be performed using transmission microscope in scanning mode. The spatial mapping in EELS provides the EM-LDOS mainly in the direction along the electron beam axis similarly to CL measurements. Dark plasmonic modes can thus be detected by EELS.⁹⁰ Compared to CL, EELS signal is very intense. As a consequence it is possible to work with rather low electron current to avoid any damage on the sample. In addition it is not necessary to enlarge the electron beam to measure a detectable signal and the spatial resolution can thus be improved.

Once again the beam diameter is not the only parameter influencing the final spatial resolution: the range of effective interaction with the sample can be much larger. For a 100 keV electron beam this range can reach 10 nm, a value much higher than the typical size of the electron beam. Further technical developments will help improving this value but some factors such as radiation damage, delocalization of inelastic scattering and beam broadening in the sample will remain as experimental limitations.⁹¹

Typical mapping using EELS signal can be seen in Figs.3(B,C). In the first study gold triangular bowtie nanostructures were prepared using high resolution electron beam lithography (Fig. 3(B)).⁹² The mapping was obtained by integrating EELS signal intensity over various energy ranges. The authors clearly indicate that even if these maps do not represent the exact photonic density of state, they are yet strongly related to the plasmonic modes of such nanostructures. The second EELS study is performed on a bent silver nanowire (Fig. 3(C)).⁸⁹ Different modes are clearly evidenced and compared to calculated EELS signal and FDTD simulations. It must be noticed that since EELS is a pure electronic process, the control over the input or output polarization is not possible. This makes the comparison with pure optical images rather complicated. It must be pointed out that there is no clear theory linking EELS and optics and the final interpretation of EELS mapping of plasmonic nanostructures is still a field of intense research.^{93, 94} In Fig. 3(C) it should be noticed that calculated EELS signal and optical FDTD simulations do not give exactly the same images. This confirms that the relation between optical properties and electronic measurements is not straightforward.

Recent developments in electron microscopy. To improve the compromise between spectral and spatial resolution, new methods based on transmission electron microscopy are currently under development. They can be more or less seen as a variation of EELS measurements. The approach is based on the combination of high spectral resolution of optical probes with high spatial resolution of electrons beam.⁹⁵ The development of time resolved electron microscopy appears as extremely promising for the study of plasmonic nanostructures.⁹⁶ In this context, photon-induced near-field electron microscopy (PINEM)⁹⁷ is a promising technique. In PINEM, the metallic nanoparticle is excited with a photon coming from a femtosecond laser and, simultaneously, an ultrashort electron pulse images the near-field induced by the optical excitation. An example of an image obtained with this technique can be seen in Fig. 3(D).⁹⁸ Different modes from close packed silver circular nanoparticles are thus evidenced. A very important advantage of PINEM over EELS is that it is possible to control the polarization of the optical excitation. Similar to CL and EELS, the recorded field is the component along the direction of the electron beam. The major drawback is that it requires a rather sophisticated TEM equipped with a femtosecond laser system and a post-column energy spectrometer.

As a conclusion for electron microscopy techniques used to map the near-field properties of plasmonic nanostructures, EELS and CL appear as extremely promising and complementary: CL offers a very good spectral resolution whereas EELS offers a very good spatial resolution. Ultimately, the best solution is to have access to both methods, which is technically possible but requires a very sophisticated and thus costly microscope. In addition the necessity for the sample to be transparent to electron beam is a major drawback for the use of a TEM for the study of plasmonic nanostructures. The final information given by these techniques is still under discussion even if it appears that it is strongly related to the out-of-plane EM-LDOS. Some dark modes can thus be observed but hot-spot with very intense in plane electric field can hardly be detected. Electron microscopy techniques are thus perfectly complementary to optical techniques.

PHOTOEMISSION ELECTRON MICROSCOPY

Photoemission electron microscopy (PEEM) methods have been used to probe the resonances in the vicinity of metallic nanostructures by collecting the electron emission induced by the irradiation with a far-field source such as tunable femtosecond laser pulse (Fig.1(C)). The brightness of the collected image corresponds to the area with larger photo-emitted electron flux.⁹⁹⁻¹⁰¹ The source of electron emission results from a cascade photo absorption process due to the formation of electron-hole pairs within several femtosecond upon excitation. Such hole-pair formation is confined in the near-field vicinity of the metallic structure, and provides a direct evidence of the plasmon enhancement with a resolution limited by the electron optics (i.e. in the range of 20-40 nm). Nevertheless other mechanisms may interfere with the electron emission such as field-emission, photoemission, thermo-ionic emission and other nonlinear optical processes. The measure must be carefully analyzed to provide unambiguous information on the localized surface plasmon. For possible nonlinear optical phenomena, measurements as a function of the input laser power shall be conducted to estimate the power dependence of the emitted electron flux. The interest of using short pulses and high repetition rate lasers opens the possibility to localize the plasmon modes and study their coupling with the metallic structure, to excite them with a selected polarization^{102, 103} as well as to study their dynamics.¹⁰⁴

In the work of Hrelescu et al.,¹⁰² selective excitation at the tips of gold nanostars was performed by tuning the polarization and the wavelength of a femtosecond Ti:sapphire laser under grazing incidence angle (75 degree with respect to the surface normal). The femtosecond excitation source was tunable in the 720-940 nm range and its polarization adjusted at selected angles with respect to the p-polarization. The imaging of the photoemitted electron was performed using a combination of PEEM, low energy emission (LEEM) and SEM. The nanostars have dimensions in the range of 100-200 nm as imaged by SEM (Fig. 4(A(a))) and are deposited onto an ITO substrate.

PEEM imaging of an individual nanostar under selected polarization and excitation wavelengths yields a composite image where the tips of the single nanostar can be selectively excited and superimposed with the SEM image (Fig. 4(A(b,c))). For a given excitation wavelength set at 860 nm, the hotspot can be selectively excited by switching the input polarization from p to p-72° as shown in Figs. 4(A(d,e)). Changing the excitation wavelength to 760 nm allows to excite another individual tip of the nanostar (Fig. 4(A(f))) while combination of wavelength and polarization can yield to the excitation of several hot-spots simultaneously (Fig. 4(A(g))). The combination of such ensemble of experiments performed at variable wavelengths and polarization reported in Fig. 4(A(h)) yields a complete photoemission map that can be correlated with the geometry of the actual nanostructure.

In addition to tuning the input polarization of the exciting beam, the control of the phase between transverse electric and magnetic polarizations has been carried on gold bowties fabricated over ITO surface using PEEM together with field modelling. Size of the individual triangles was set to 350 nm while large gap of 100 nm was used (Fig. 4B(a)). The photoemission pattern was collected for one-photon emission upon excitation at 253 nm to localize the nanotriangles collective resonance. For three-photon excitation at 800 nm, the confined hot-spot was clearly observed at the gap between opposed nanotriangles. As highlighted in Fig. 4(B(b,c)), the patterns are clearly polarization dependent and stronger confinements are observed when the polarization is along the bowtie axis (TM mode, Fig. 4(B(b))) while external tips of the left triangle shows dimmer confinement when the polarization is orthogonal to the bowtie axis (TE mode, Fig. 4(B(c))). Such experimental results obtained with a 40 nm resolution are corroborated by field modeling. When both TE and TM excitation are used simultaneously, the manipulation and the switching of the resonances in a single bowtie assembly can be performed by controlling the phase between the two orthogonally polarized laser pulses which yields a PEEM pattern that reveals near-field interferences. The tips of the gold triangle can be selectively excited by tuning the phase between the TE and TM polarizations as shown in Fig. 4(C).¹⁰⁵

Imaging of the plasmon dynamic modes was investigated by combining PEEM and interferometric time-resolved two-photon photoemission pump-probe experiments yielding maps of the surface plasmon modes in silver gratings with sub-femtosecond resolution and sub-wavelength spatial resolution.¹⁰⁴ Although this work was published as early as in 2005, it is still of particular interest in the context of this focal point. Using an excitation set at $\lambda=400$ nm and with pulse of 10 fs, the E^4 dependence of the emission confirms the second-order nonlinear resonance revealed by some surface plasmon resonances localized around protusions in the silver grating (Fig. 4(D(a))). The dynamics of the selected resonances was investigated dynamically by adjusting the delay between the pump and the probe with intervals as small as 330 attoseconds yet

keeping a spatial resolution better than 50 nm. Interference of the electron oscillation with the excitation light source change depending of the pump-probe delay, highlighting the collective oscillation at the optical carrier frequency and their dissipative relaxation once the pulse is passed. The pump-probe experiments show clear evolution of the interference pattern depending on the delay between the pump and the probe revealing the dynamics of the localized surface plasmons as shown in Fig. 4(D(b)). Importantly, this approach opens full access on the spatiotemporal evolution of the plasmon modes by controlling the phase of ultrafast laser sources which in turns paves a new way to study coherent excitations of localized or propagative plasmon modes. However, any other optically induced phenomena must be carefully considered for the analysis of the images and control experiments using distinct wavelength may be of importance to rule out specific phenomena.

In conclusion, PEEM presents key advantages to probe the dynamics of plasmon resonances or the effect of polarization of the impinging excitation with a spatial resolution in the 20-50 nm range. It eliminates the perturbation from a local probe such as a NSOM or an AFM tip in the near-field of the sample and provides background free images allowing a comprehensive statistical analysis of the hot-spots, of their distribution and their associated resonance wavelengths. More importantly such technique allows one to not only visualize plasmon resonances at selected wavelength but also to manipulate their spatial confinement using interferometric scheme in the excitation. Limitations of the technique arise from grazing angle of incidence on the sample and impossibility to analyze the polarization of the emitted electron beam. Correlation of PEEM results with nonlinear optical measurements (two-photon induced luminescence, second harmonic generation) using the same tunable light source will be of great interest to better characterize the LSPR.

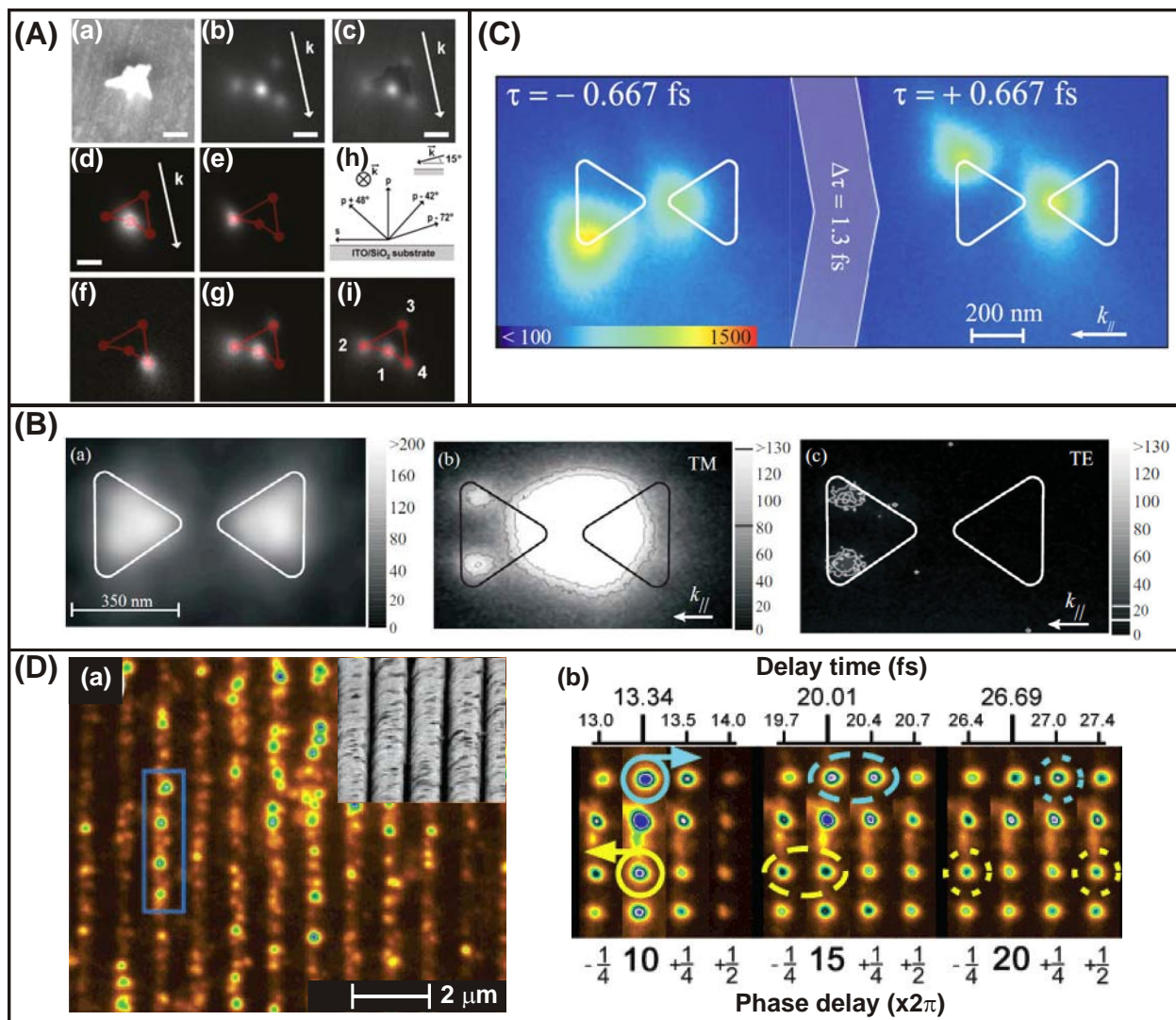


Fig. 4. (A) Selective excitation of individual tips of a gold nanostar. SEM, PEEM and composite images of an isolated nanostar (a,b,c). (d,e) PEEM under 860 nm excitation with p and p-72° polarized excitations, respectively. (f,g) PEEM under 760 nm excitation with p+48° polarization and 860 nm with p-42° polarizations, respectively. (h,i) polarization diagram of the input source and composite image created with selected input polarization and excitation wavelengths. (Adapted with permission from ref.102. Copyright 2011 American Chemical Society). **(B)** Photoemission of the bowtie antenna using 1 photon excitation (a), 3 photon excitation with TM polarization (b) and TE polarization. (Reprinted with permission from ref. 105. Copyright (2011) by the American Physical Society). **(C)** Switching of the local resonances by adjusting the delay between the two laser pulses. (Reprinted with permission from ref. 105. Copyright (2011) by the American Physical Society). **(D)**(a) two-photon photoemission from a silver grating with p-polarized input. (b) Sequence of interferometric time-resolved photoemission of four localized Plasmon. The delay between the pump and the probe is adjusted, allowing one to finely tune the phase of the surface plasmon mode with respect to the impinging field as highlighted in the circled areas. (Adapted with permission from ref. 104. Copyright 2005 American Chemical Society).

IMAGING PLASMONS WITH NON-LINEAR OPTICAL PHENOMENA.

Due to local enhancement of the electric field in the vicinity of metallic nanostructures, the application of plasmonics to nonlinear optical measurements is of great interest since the field will be enhanced significantly. Conversely, this local enhancement that varies nonlinearly with the input power can be used to map hot-spots present in the plasmonic structures. The spatial resolution of the optical measurement depends on the type of microscopy used, namely near-field or far-field microscopes. In far-field measurements, the nonlinear optical measurements will have a typical spatial resolution in the ~200 nm range.

In nonlinear processes, the response of a material to an optical field \mathbf{E} is described by the materials polarization \mathbf{P} that can be expanded in a series that includes the linear and the nonlinear contributions:

$$P = \epsilon_0 [\chi^{(1)}: E(\omega) + \chi^{(2)}: E(\omega_1)E(\omega_2) + \chi^{(3)}: E(\omega_1)E(\omega_2)E(\omega_3) + \dots] \quad (1)$$

The $\chi^{(1)}$ and $\chi^{(n)}$ denote the linear and nonlinear susceptibilities, respectively, that are related to the complex amplitude of the electromagnetic field for a given set of input/output polarizations. ϵ_0 is the vacuum permittivity.

For second harmonic generation (SHG), if the medium has inversion symmetry then its susceptibility $\chi^{(2)}$ will vanish under the electric dipole approximation. For plasmonic platforms with shapes that have no inversion symmetry, the $\chi^{(2)}$ is non-zero and will yield second order signal. Furthermore, since the output field varies quadratically with the input field, a small increase of the local field will lead to a large increase of the SHG signal. Other nonlinear phenomena such as sum frequency generation (SFG, $\chi^{(2)}$ process) or coherent anti-Stokes Raman scattering (CARS, $\chi^{(3)}$ process) can presumably benefit from such local enhancements as long as the resonances of the metallic structures match the spectral range of the excitation input and output fields. Little work has been conducted on plasmon-enhanced nonlinear spectroscopy. Such effect will be more drastic for higher order nonlinear phenomena (Third harmonic, CARS) enhancing greatly signals that are typically weak.³⁰ Reciprocally, since the output field is nonlinearly enhanced with respect to the input field, its localization is presumably even more confined and such optical nonlinear effects can therefore be used to map LSPR over plasmonic platforms with excellent spatial resolution.

When subject to intense laser pulses, higher order susceptibilities such as $\chi^{(2)}$ or $\chi^{(3)}$ are involved, revealing sum, differences and combinations of the incident frequencies. Such third and fourth rank tensors contain individual susceptibilities terms that are can be probed individually by properly selecting the incident polarization(s) as

well as the polarization of the output beam(s). Furthermore the $\chi^{(i)}$ is dependent on the symmetry and/or orientation of the object that generates the output field. In the specific case of second-order nonlinear processes, non-centrosymmetric metallic structures or nanocavities inscribed in a metal film are prerequisites yielding a polarized SHG pattern, the shape of which depends on the symmetry of the considered structure or assembly.¹⁰⁶ It was also shown that the amplification of SHG can indeed be suppressed at the gaps between adjacent structures which appear to be dependent on the local symmetry of the structure. The presence of an inversion center will cancel second order nonlinear optical signal. In such case, electromigration process was used successfully to break the symmetry of the gap morphology between adjacent single antennae yielding larger nonlinear response.¹⁰⁷

Beyond the applications of nonlinear plasmonics, several studies have made use of plasmonics platforms fabricated by electron-beam lithography to enhance second order nonlinearities.¹⁰⁸ SHG far-field microscopy (Fig. 1(C)) was first applied to probe G shape Nickel structures revealing the area with the highest field enhancement located at the extremities of the structures for a selected polarization and irradiance (Fig. 5(A(a-c))). Above a certain threshold of intensity, the structures are locally melted by the fs pulses as seen by SEM and AFM after irradiation (Fig. 5(A(d))). The input polarization direction is also critical for the development of the hotspot in particular for anisotropic structures such as nanobricks. The melted area reveals the hot-spots of the structure while no drastic temperature changes are observed in the rest of the structure.¹⁰⁹ Application of SHG circular dichroism to probe chiral plasmonic structures have been highlighted using G shape structures with left and right handedness.¹¹⁰ In this work, the SHG microscopy maps generated with a circularly left or right input light yielded distinctive distributions of hot-spots depending on the handedness of the structure (Fig. 5(B)). The use of these chiral metastructures is of particular interest for sensing of chiral biomaterials such as DNA or RNA that would presumably adsorb distinctively over the chiral metallic structures.

Two-photon induced luminescence (TPL) and fluorescence (TPF) are third order nonlinear optical processes that vary quadratically with the excitation power.¹¹¹ In TPL and TPF, the nonlinear absorption of the two input photons populate the first electronic state of the irradiated material which relax through fluorescence or luminescence processes. This is a distinct physical process compared to SHG process where the two photons induce a change in the polarization of the material. Since TPL and TPF processes are governed by a $\chi^{(3)}$, there is no pre-requisite on the symmetry of the plasmonic material to yield a TPL or TPF signal.

TPL was used to probe field distribution in asymmetric gold bowtie assemblies,¹¹² and in gold prismatic nanoplates made by chemical synthesis (Fig. 5(C)).¹¹³ Such

ultraflat nanoplates have a roughness in the range of 500 pm and were used as substrates of choice for tip-enhanced Raman spectroscopy that also benefits from the excitation of LSPR at the extremity of a metallic tip.^{114, 115} In this study, the influence of the input polarization and wavelength were investigated to reveal the surface plasmon local density of photonic states. Small variation in the orientation of the input linear polarization allows one to control and switch the luminescence at the individual three apices of a single gold nanotriangle as shown in Fig. 5(C(a-f)). Circular polarization results in a uniform TPL signal distribution across the triangular nanoplate. This opens new possibilities involving single plasmonic particles as logic nano-architectures for optoelectronics applications.¹¹³ Other geometric structures shown in Fig. 5(D(a-c)) were investigated by TPL such as structures made using capillary forces to fabricate a variety of structures with distinct opto-geometric properties highlighting the polarization dependence on the TPL maps.¹¹⁶

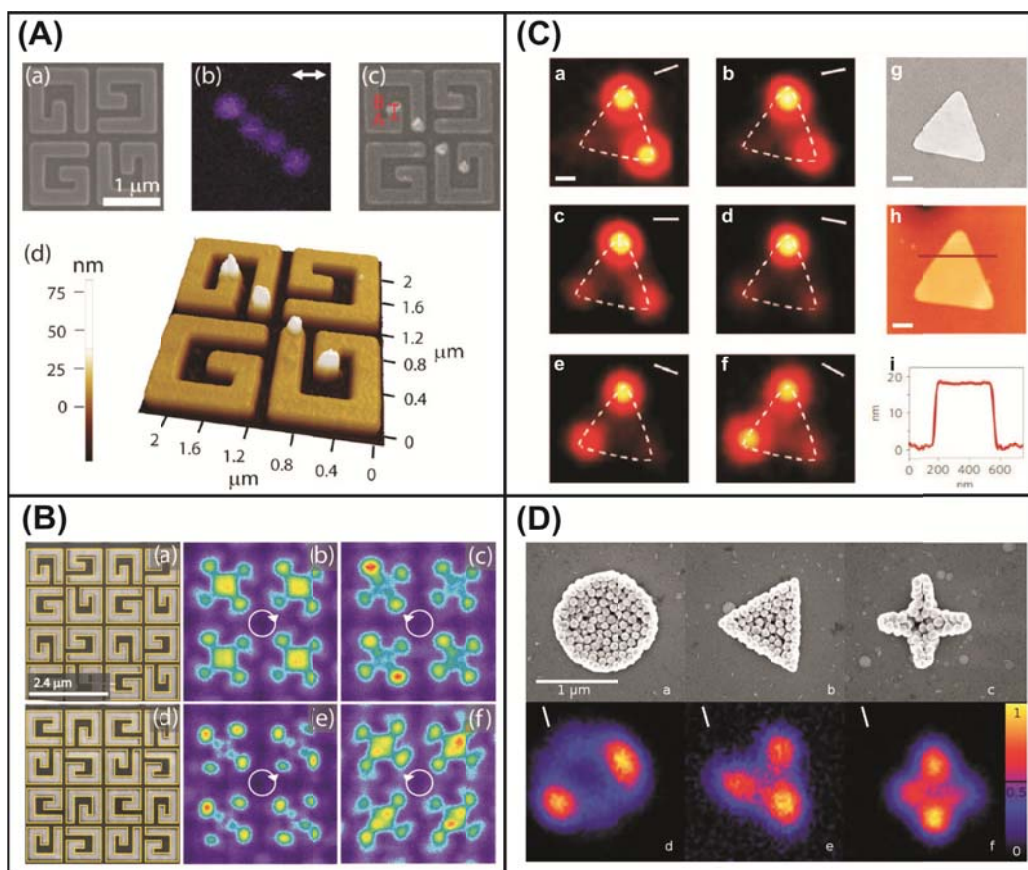


Fig. 5. (A) G-shape Nickel nanostructures on SiO₂/Si(001) substrate (a). SHG signal (b) and SEM image after irradiation (c). The AFM image shows photoinduced damages at the extremities of the structures provided when the polarization is oriented along the gap formed by the extremities of a given structure (d). (Reprinted with permission from ref. 109, Copyright (2011) by the American Physical Society) (B) SHG responses from chiral structures (a,d) using circularly right (b,e) and left (c,f) polarized input fields. (Adapted from ref. 110 with permission of American Chemical Society, Copyright 2012) (C) Two-photon induced luminescence (a-f) from ultraflat gold flakes (g-

i). The TPL signal can be tuned by small changes of the direction of the input linear polarization. (Reprinted from ref. 113 by permission from Macmillan Publishers Ltd: Nature Materials, copyright (2013)) (D) TPL signal from assemblies of gold nanoparticles made by capillary convection forces method (a-c) and their associated TPL signal for a given excitation polarization (Reprinted with permission from ref. 116 Copyright (2013) by the American Physical Society).

In conclusion, the investigation of plasmonic platforms with well defined shapes and symmetries using nonlinear optical processes is an emerging field that can lead to improvements in sensitivity and spatial resolution in nonlinear spectroscopy and microscopy as well as help to manipulate light properties at the nanoscale for further applications such as in chiral-sensing, high-resolution optical microscopy or logic gates. The possibility to probe the LDOS using TPL provides unvaluable informations that are difficult to obtain with electronic microscopy techniques described in the previous paragraphs. Finally, information on plasmon lifetime provided by time-resolved experiments would allow one to evaluate the rates of the distinct processes mediated by plasmon excitation opening new prospectives in the field of plasmonic light sources.¹¹⁷

INDIRECT IMAGING METHODS

Indirect imaging methods exploit physical, chemical or spectroscopic photoinduced local changes or singularities in the vicinity of metallic nanostructures (Fig. 1(D)) Such photoinduced changes can be observed using imaging methods such as SEM, atomic force microscopy (AFM) or spectroscopic techniques such as Raman or infrared microscopy. AFM probes can serve to sense the local optical forces exerted by a LSPR.

Thermally enhanced effects can be observed in plasmonic structures when the resulting enhanced local field is close to the melting threshold of the metallic structure. Under ultrafast laser irradiation, subsequent heating and melting can be observed when high irradiance is used. This is presumably due to the confined and thermal gradient around the nanostructure due from the short thermal diffusion yielding to thermal effects on length scales smaller than the dimension of the object. G shape Au/Ni/SiO₂/Si structures are nice examples where the formation and the ejection of metal droplet can be visualized at the extremities of the structure (Fig. 6(A)) where the field is the most intense as predicted by FDTD modeling and observed by SHG measurements.¹¹⁸ Post-irradiation imaging of these structures by SEM shows that the local field can be used to fabricate and manipulate metallic nanoparticles when thermal effect are involved. Thermal effects were investigated on nanosphere lithography substrates.¹¹⁹ Using pulsed fs source and fluence varying from 70 mJ/cm² to 370 mJ/cm², local thermal modification of the individual nanotriangles could be revealed by SEM using polarizations along or orthogonal to a triangle axis. This study suggests that the interaction of similar structures with a radially or an azimuthally polarized light could be

of interest by allowing one to probe distinct elements of the material susceptibility tensor.

An elegant way to image hot-spots in plasmonics surfaces is to use photosensitive thin film deposited over the plasmonic surface that will undergo selective chemical or physical change upon irradiation. Since the local field is larger in the vicinity of the metallic nanostructures, one can expect a faster or more efficient change in the properties of the photosensitive material. Photopolymerizable formulation is a nice example of material that will be more efficiently polymerized in the hot-spots. For such material, the threshold of the laser dose and the irradiation time must be well determined to avoid polymerization of the whole thin film deposited over the metallic structures. As reported by Bachelot et al. for a formulation sensitized with a dye absorbing the excitation wavelength, short irradiation time of 2 seconds and irradiance set to 2 mW/cm^2 at 514 nm is sufficient to display large topographical changes up to 30 nm of the polymer surface as monitored by SEM or AFM.¹²⁰ This approach offers a unique and easy method to probe the optical near-field of silver nanoparticles and was applied to tip-enhanced microscopy where the optical field underneath a metallic AFM tip was probed using similar polymer formulation.¹²¹

Common polymers used in photo- and electron beam-lithography processes can also be used. For example, Misawa et al. used a 70 nm layer of commercial positive (TSMR V-90) photoresist to image the optical near-field in the vicinity of gold nanocubes dimmers.¹²² When the polarization of the input 800 nm Ti:sapphire laser is oriented along the long axis of the dimmers, photopolymerization occurs at the gap whereas it occurs along the minor axes of the cubes corners when the polarization is set orthogonal to the gap axis. Estimation of the enhancement factor was provided using FDTD modelling but it should be possible to determine it experimentally knowing the threshold dose of the resist together with the irradiance and irradiation time of the assembly. Quidant et al. have reported on the four photon absorption in PMMA-embedded gold nanorods.¹²³ Using a tunable Ti:Sapphire laser with incident powers in the range of hundreds of microwatts and exposure time of 30 s, the snapshots of the near-field enhancement can be imaged using SEM after developing the exposed polymer film (Fig. 6(B)). The input wavelength can be tuned depending on the antenna length and its plasmon resonance wavelength in the near-infrared spectral range. Imaging of a series of isolated gold nanoantennas with distinct lengths was performed highlighting precisely the different modes that are dependent on the length of the individual rods and excitation wavelength. The mapping of gap antennas indicated a clear confinement at the junction between the gold rods under weak illumination conditions while higher intensities lead higher resonant modes along the antenna.

Of interest, functionalized polymers with pendant azobenzene groups, are particularly well suited to study the electric field intensity distribution because of their

self-developing properties. When irradiated with a linearly polarized light with a wavelength that matches the absorption of the azobenzene moieties, a stable surface topography change is observed at room temperature without any developing step which makes it a system of choice to reveal areas where the input field is locally intensified. Several groups have made use of azopolymers thin films to image the spatial distribution of the enhancement nearby a metallic structure such as a metallic AFM tip¹²⁴ or arrays of metallic nanostructures deposited onto a surface.¹²⁵⁻¹²⁸ The photoinduced deformation being stable after irradiation, atomic force microscopy is a technique of choice to probe surface changes with nanometer resolution. The effect of the polarization has been conducted on regular arrays of plasmonic platforms fabricated by electron-beam lithography,¹²⁵ nanosphere lithography¹²⁸ and correlated with field simulations. These results are of interest to localize the areas where the field is strongly enhanced by measuring the changes of topography such as those observed in tetrahedral silver nanopylramids made by nanosphere lithography (Fig. 6(C(a))).¹²⁸ Figs. 6(C(b,c)) show the AFM profiles along two cross sections. For two adjacent pyramids the change of topography before and after irradiation with a cw 532 laser with an irradiance of 100 mW/cm², shows small variations with amplitudes ranging between 3 and 10 nm depending on the considered dimer formed by two pyramids. These results must be however carefully discussed since the orientation and photomigration of azopolymer is dependent on the type of azopolymer thin film used in the study (amorphous, semi-crystalline, liquid-crystalline) as well as the molar ratio of azobenzene moieties in the polymer chain. Uniaxial or biaxial orientation can be observed depending on the functionalization or doping level and associated photoinduced migration can be different. Biaxial orientation is reported for highly charged polymer and, in the context of imaging individual hot-spots must be carefully analyzed. The thin film is then irradiated with a wavelength that matches both the electronic resonance of the azobenzene moieties and the LSPR of the nanostructures. More recently, Koenig et al. have made use of gold plasmonic platforms made by nanosphere lithography to study the change of topography of a thin film of an azobenzene containing a polyelectrolyte sensitive to humidity. Upon the change of humidity, reversible changes of topography were evidenced by AFM providing spatial informations on the plasmon resonances.¹²⁹

Vibrational spectroscopy was also used to probe the near-field enhancement in the vicinity of gold antenna. Dregely et al. made use of patches of probe molecules accurately placed at the nanoantenna gaps or extremities. In a dual electron-beam procedure, (200x200) nm² patches of hydrogen silsesquioxane were placed within a 10 nm accuracy over specific positions over the antenna preliminary fabricated over CaF₂ windows. The vibrational mode of Si-H (2252 cm⁻¹) was collected in transmittance using a FTIR microscope equipped with a Cassegrain objective. The strength of the vibrational signal measured at various positions along the gold rods and was in good agreement with the modelling of the near-field enhancement. More complex 3D buried

plasmonic structures were also investigated showing the strength of this approach. It is noteworthy that considering the poor spatial resolution of a typical infrared microscope (in the range of several microns), the strong coupling between the molecular vibrations and plasmonic resonances allows one to detect a strong signal confined at a defined position over a metallic structures with an excellent spectral resolution. Such approach conducted with focal planar array detectors would be of great interest to map vibrational resonances over larger and more complex metallic nanostructures and could be extended to the Terahertz spectral range.¹³⁰

Confocal microscopy coupled to Raman as well as fluorescence measurements were successfully used on functionalized nanohole and nanotriangle gold arrays. The superimposition of a Raman SERS map of a thiolated molecule with the topography measured by atomic force microscope of the same plasmonic platform was used to map the areas where maximum Raman signal was collected and determine optimized hole size and periodicity for maximum enhancements for a given input polarization.^{21, 131} For surface enhanced fluorescence measurements, a solution of fluorescent was used over silica protected nanotriangles arrays.²⁵ The fluorescence pattern revealed the position of the hot-spots formed by pairs of bowtie assemblies. In these experiments the lateral resolution is spatially limited to $\lambda/2$ according to Abbe's criterion while non-linear optical microscopy measurements have a better spatial resolution due to a tighter confinement of the excitation source.

The extreme sensitivity of an AFM cantilever subject to small forces was used to probe the near-field in a single bowtie assembly.¹³² The single nanoantenna layered structure of Au/SiO₂/Au (with respective thicknesses of 40/30/40 nm) was made on the facet of an optical fiber. (Fig.6(D), top) Once the incoming excitation light ($\lambda=1550$ nm) was injected from the other opposite facet of the fiber, the incident light focuses down to a spot that is smaller than the incoming field by several orders of magnitude. For a input polarization along the bowtie axis, the light is focused between the two individual gold triangles separated by a 50 nm gap. When an AFM tip is in interaction with such optical trap, the cantilever senses the local near-field forces that are in the 0.6 pN range (Fig. 6(D), bottom). For an input polarization orthogonal to the bowtie axis, no optical force is detected highlighting again the drastic polarization conditions to excite a localized LSPR in such anisotropic structures. For an optimized cantilever with a spring constant of 3 N/m, a quality factor of 160 and resonance frequency of ~ 100 kHz, force sensitivity as small as 40 femto Newton is expected opening optical near-field sensing measurements with an apertureless setup for a variety of applications ranging from biosensing to optical switching.

In conclusion, a variety of indirect methods using photosensitive thin films or functionalized plasmonic surfaces have been successfully demonstrated to map the distribution of hot-spots over plasmonic surfaces. These approaches are required to determine accurately the threshold dose to reveal the hot-spot which implies that a

series of experiments must be preliminary conducted. The use of an AFM probe provides resolution in the nm range revealing subtle surface deformation mediated by LSPR. Last, the sensitivity of AFM cantilevers to optical forces is an elegant approach to reveal the distribution of hot spots. Lateral or normal oscillation of the tip should provide detailed information on the polarized components of the LSPR modes.

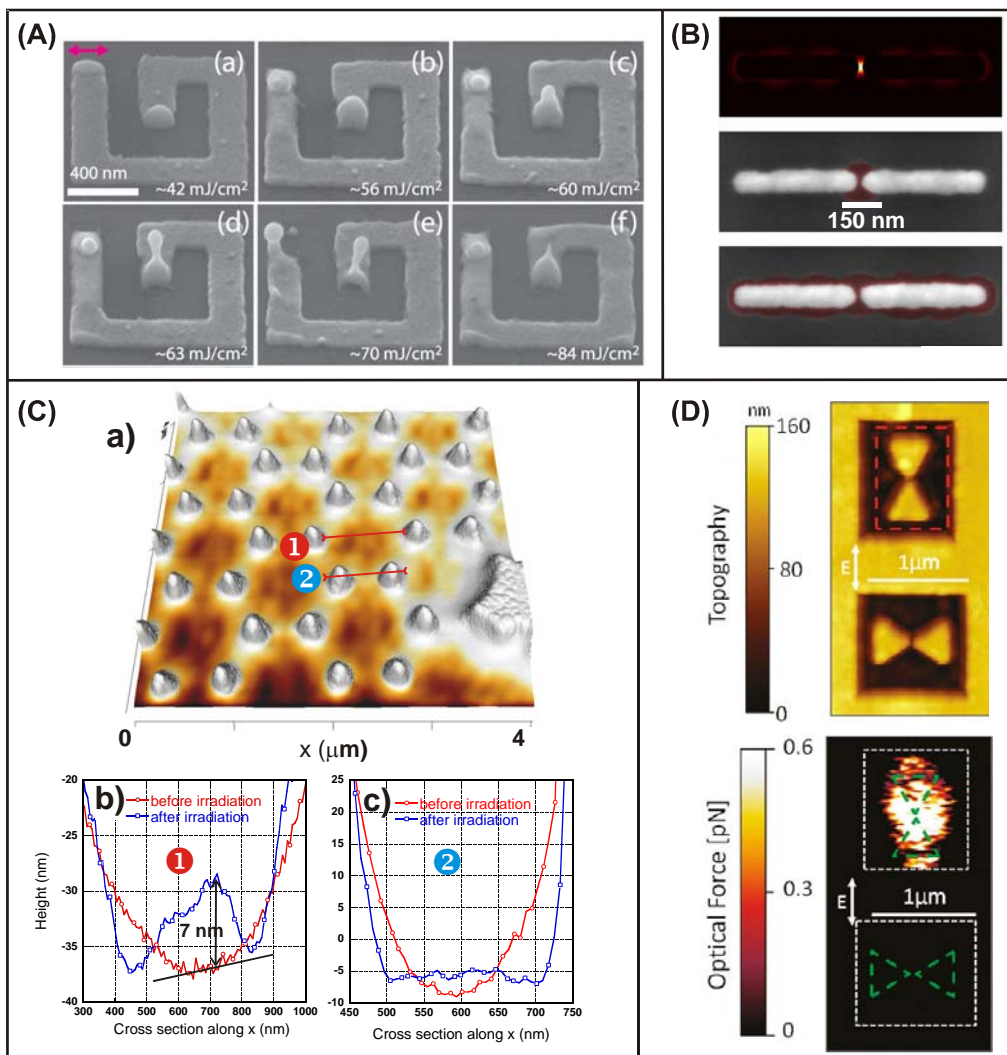


Fig. 6. (A) Formation (a-e) and ejection (f) of a Au nanodroplet by plasmon-induced thermal effect in a G shape gold structure. (Adapted from ref. 118 with permission of John Wiley and Sons, Copyright 2012). (B) Monitoring LSPR modes in a single antenna using a thin film of polymethylmetacrylate. At low intensity the confined field is observed at the gap as expected by FDTD calculation (top-middle) while at larger intensities the distinct plasmon modes can be observed experimentally along the antenna. (Adapted from ref. 123 with permission of American Chemical Society, Copyright 2012) (C) Nanosphere lithography silver nanopyramids coated with a thin film of azopolymer after irradiation at $\lambda=532 \text{ nm}$ (a). The variations of the topography can be measured along the cross sections at the gap between adjacent pyramids (b) or along the center of the unit lattice (c). In both cases changes of topography indicate photoinduced mass-transport

mediated by the LSPR of the metallic structure. (Adapted from ref. 128 with permission of American Chemical Society, Copyright 2013). (D) Bowtie antennas made of Au/SiO₂/Au on the distal facet of an optical fiber (top). Optical force detected by the AFM probe in the optical near-field of the bowties (bottom). (Adapted with permission from ref. 132 with permission of American Chemical Society, Copyright 2012).

Table I. Summary of the main techniques used to probe localized surface plasmons on metallic nanostructures.

Technique	Process	Resolution limit	Advantages	Disadvantages
Scanning near-field microscopy	Photon in-Photon out (Aperture or Apertureless)	~10-50 nm (diameter of the probe)	Simultaneous optical contrast and topography Can be coupled with a variety of optical processes. Control of polarization for both excitation and emission. Pure optical measurement.	Reproducibility and wear of the scanning tip. Complex analysis of the optical near-field images due to the tip-sample interaction. Low signal to noise ratio (requiring for some measurements complex detection techniques to increase this ratio). Measurements are usually performed for a single excitation wavelength (laser source).
Cathodoluminescence	Electron in-Photon out (SEM or TEM)	~20 nm Slightly higher in transmission electron microscope	It is possible to perform both spectral and spatial measurements. Very high spectral resolution (~1 meV) . High spatial resolution typically a few nm. Dark modes can be detected.	Control of polarization only for the emitted light. High vacuum measurement. Samples must be conductive. The electron beam can damage the sample (ex: carbon deposition). Signal to noise ratio rather low.
EELS	Electron in-electron out (TEM)	~10-20 nm	Very high spatial resolution. High spectral resolution (~100 meV) High signal-to-noise ratio.	No control of the polarization. High vacuum measurement. Only for thin samples transparent to electron beams . The lowest energy measurable is limited by the intense

				elastically transmitted electron beam. High energy electron beams (200-300 kV) can damage the sample.
PEEM	Photon in- Electron out	~10-20 nm	In-situ irradiation and detection in UHV conditions. Can be combined with low energy electron microscopy No interaction with a perturbative near-field probe in the vicinity of the object. Polarization of the input light can be controlled. Background free technique.	Angle of incidence of the light source is limited. Need for a conductive substrate. Tunability of fs source is required.
Non-linear optical microscopy	Photon in- Photon out	~200 nm	Full control of the input/output polarization. Provides information on the symmetry and orientation of the nanostructure. Versatile measurements in multiple configurations (transmission, reflection) and combination to near-field or far-field microscopy	Symmetry of the plasmonic structure is critical for efficient non-linear optical processes. Laser pulses can damage the metallic structures. Tunability of the input wavelength requires amplifier and optical parametric oscillator.
Indirect Imaging methods	Photosensitive material	~5-20 nm depending on the material used and associated measurement	High resolution of the measurement using atomic force microscopy or electronic microscopy. Possibility of in-situ irradiation	Threshold of the exposure must be first determined to reveal local hot-spots. Ex-situ measurements. Materials can be sensitive to the polarization of the impinging light leading to anisotropic topographical changes

FINAL REMARKS

The study of the optical near-field of plasmonic nanostructures has led to the development of a wide variety of experimental tools. Each technique offers its advantages in terms of spectral and spatial resolution, polarization control and time analysis as summarized in Table I. Of course, these features are obtained at the cost of several drawbacks such as costly experimental apparatus, ultra-high vacuum measurements, preparation of the samples or the near-field probes. The rapid pace of technical developments for these techniques will with no doubts help improving the limitation and the signal quality. In addition, new techniques or developments will probably emerge in the future.

Nevertheless all these approaches have a common point: the final interpretation of the recorded image is not straightforward mainly because of the complex and sometimes unclear probe-sample interaction. As a consequence in most of the reported near-field studies, experimental results are compared with numerical simulations. Optical modeling tools are thus absolutely necessary for the complete comprehension of the optical near-field measurements. They are ideally complementary to experimental studies.

Finally, a question still remains: what is the best technique to study the near-field of plasmonic nanostructures? Comparing the different methods presented in this focal point, it appears clearly that it is impossible to answer such a question. As mentioned above, each approach offers its advantages and limitations. As a consequence the different techniques are perfectly complementary instead of being in competition. If we push forward this argument, it appears that the complete knowledge of a given plasmonic nanostructure will require a wide range of measurements, each of them bringing specific information. So far, very few studies have taken advantages of the fact that these techniques and associated expertise are complementary. In addition to the fabrication of the nanostructures, it is not surprising that very little number of research laboratories and university facilities can gather all these techniques and associated skills in a single place. As a consequence the further understanding of plasmonic nanoantennas will absolutely require putting those skills in common and thus strong collaborations. This is a major challenge for our community.

ACKNOWLEDGMENTS

This research was funded by the Natural Sciences and Engineering Research Council of Canada Discovery Grant and by the Canada Research Chairs program. The authors

also acknowledge the Agence Nationale de la Recherche Scientifique (ANR) for financial support under the CARIOCA project (2010-JCJC-918-01).

REFERENCES

1. H. Caglayan, S.-H. Hong, B. Edwards, C. R. Kagan, N. Engheta. "Near-infrared metatronic nanocircuits by design". *Phys. Rev. Lett.* 2013. 111(7): 073904.
2. J. R. Cole, N. A. Mirin, M. W. Knight, G. P. Goodrich, N. J. Halas. "Photothermal efficiencies of nanoshells and nanorods for clinical therapeutic applications". *J. Phys. Chem. C* 2009. 113(28): 12090-12094.
3. X. Huang, M. A. El-Sayed. "Gold nanoparticles: Optical properties and implementations in cancer diagnosis and photothermal therapy". *J. Adv. Res.* 2010. 1(1): 13-28.
4. M. Sun, H. Xu. "A novel application of plasmonics: plasmon-driven surface-catalyzed reactions". *Small* 2012. 8(18): 2777-2786.
5. H. A. Atwater, A. Polman. "Plasmonics for improved photovoltaic devices". *Nat. Mater.* 2010. 9(3): 205-213.
6. P. V. Kamat, G. C. Schatz. "Nanotechnology for next generation solar cells". *J. Phys. Chem. C* 2009. 113(35): 15473-15475.
7. A. G. Brolo. "Plasmonics for future biosensors". *Nat. Photonics* 2012. 6(11): 709-713.
8. N. Liu, A. Pucci. "Plasmonic biosensors: Know your molecules". *Nat. Mater.* 2012. 11(1): 9-10.
9. S. Kawata. "Plasmonics for nanoimaging and nanospectroscopy". *Appl. Spectrosc.* 2012. 67(2): 117-125.
10. C. Valsecchi, A. G. Brolo. "Periodic metallic nanostructures as plasmonic chemical sensors". *Langmuir* 2013. 29(19): 5638-5638.
11. P. Alonso-González, M. S. P. Albella, J. Chen, F. Huth, A. Garcia-Etxarri, F. Casanova, F. Golmar, L. Arzubia, L. E. Hueso, J. Aizpurua, R. Hillenbrand. "Resolving the electromagnetic mechanism of surface-enhanced light scattering at single hot spots". *Nat. Commun.* 2012. 3: 684-690.
12. H. H. Wang, T. Y. Cheng, P. Sharma, F. Y. Chianq, S. W. Chiu, J. K. Wang, Y. L. Wang. "Transparent Raman-enhancing substrates for microbiological monitoring and in-situ pollutant detection". *Nanotechnology* 2011. 22(38): 385702.
13. B. Galarreta, M. Tabatabaei, V. Guieu, E. Peyrin, F. Lagugné-Labarthe. "Microfluidic channel with embedded SERS 2D platform for the aptamer detection of ochratoxin A". *Anal. Bioanal. Chem.* 2013. 405(5): 1613-1621.
14. A. Huefner, W.-L. Kuan, R. A. Barker, S. Mahajan. "Intracellular SERS nanoprobe for distinction of different neuronal cell types". *Nano Lett.* 2013. 13(6): 2463-2470.
15. S. S. Zhao, M. A. Bichelberger, D. Y. Colin, R. Robitaille, J. N. Pelletier, J. F. Masson. "Monitoring methotrexate in clinical samples from cancer patients during chemotherapy with a LSPR-based competitive sensor". *Analyst* 2012. 137(20): 4742-4750.
16. S. Berweger, J. M. Atkin, R. L. Olmon, M. B. Raschke. "Light on the tip of a needle: plasmonic nanofocusing for spectroscopy on the nanoscale". *J. Phys. Chem. Lett.* 2012. 3(7): 945-952.
17. J. M. Klingsporn, N. Jiang, E. A. Pozzi, M. D. Sonntag, D. Chulhai, T. Seideman, L. Jensen, M. C. Hersam, R. P. Van Duyne. "Intramolecular insight into adsorbate-substrate interactions via low-temperature, ultra-high vacuum tip-enhanced Raman spectroscopy". *J. Am. Chem. Soc.* 2014. 136(10): 3881-3887.
18. N. Kazemi-Zanjani, H. Chen, H. Goldberg, G. Hunter, B. Grohe, F. Lagugné-Labarthe. "Label-free mapping of osteopontin adsorption to calcium oxalate crystals by tip-enhanced Raman spectroscopy". *J. Am. Chem. Soc.* 2012. 134(41): 17076-17082.
19. S. A. Maier, *Plasmonics: fundamentals and applications* (Springer, New York, USA, 2007).
20. V. Guieu, F. Lagugné-Labarthe, L. Servant, D. Talaga, N. Sojic. "Ultrasharp optical-fiber nanoprobe array for Raman local-enhancement imaging". *Small* 2008. 4(1): 96-99.

21. D. Correia-Ledo, K. Gibson, A. Dhawan, M. Couture, D. Graham, T. Vo-Dinh, J. F. Masson. "Assessing the Location of Surface Plasmons Over Nanotriangle and Nanohole Arrays of Different Size and Periodicity". *J. Phys. Chem. C* 2012. 116(12): 6884–6892.
22. B. Sharma, M. F. Cardinal, S. Kleinman, N. G. Greeneltch, R. R. Frontiera, M. G. Blaber, G. C. Schatz, R. P. V. Duyne. "High performance SERS substrates: advances and challenges". *MRS Bull.* 2013. 38(8): 615-624.
23. J. M. Hoffmann, X. Yin, J. Richter, A. Hartung, T. W. W. Maß, T. Taubner. "Low-cost infrared resonant structures for surface-enhanced infrared absorption spectroscopy in the fingerprint region from 3 to 13 μm ". *J. Phys. Chem. C* 2013. 117(21): 11311-11316.
24. R. F. Aroca, D. J. Ross, C. Domingo. "Surface-enhanced infrared spectroscopy". *Appl. Spectrosc.* 2004. 58(11): 324-338.
25. S. Fayyaz, M. Tabatabaei, R. Hou, F. Lagugné-Labarhet. "Surface-enhanced fluorescence: mapping individual hot spots in silica-protected 2D gold nanotriangle arrays". *J. Phys. Chem. C* 2012. 116(21): 11665-11670.
26. H. Okamoto, K. Imura. "Visualizing the optical field structures in metal nanostructures". *J. Phys. Chem. Lett.* 2013. 4(13): 2230–2241.
27. M. Kociak, O. Stéphan. "Mapping plasmons at the nanometer scale in an electron microscope". *Chem. Soc. Rev.* 2014. 43(11): 3865-3885.
28. R. Vogelgesang, A. Dmitriev. "Real-space imaging of nanoplasmonic resonances.". *Analyst* 2010. 135(6): 1175-1181.
29. L. Douillard, F. Charra. "High-resolution microscopy of plasmon field distributions by scanning tunneling luminescence and photoemission electron microscopies". *CR. Phys.* 2012. 13(8): 815-829.
30. M. Kauranen, A. V. Zayats. "Nonlinear plasmonics". *Nat. Photonics* 2012. 6(11): 737-748.
31. D. Courjon, *Near-field microscopy and near-field optics* (Imperial College Press, 2003).
32. L. Novotny. "The history of near-field optics". *Prog. Opt.* 2007. 50(5): 137-184.
33. L. Novotny, B. Hecht, *Principles of nano-optics* (Cambridge University Press, Cambridge, 2006).
34. M. Esslinger, R. Vogelgesang. "Reciprocity theory of apertureless scanning near-field optical microscopy with point-dipole probes". *ACS Nano* 2012. 6(9): 8173-8182.
35. A. García-Etxarri, F. Romero, F. J. García de Abajo, R. Hillenbrand, J. Aizpurua. "Influence of the tip in near-field imaging of nanoparticles plasmonic modes: weak and strong coupling regimes". *Phys. Rev. B* 2009. 79(12): 125439.
36. J. Sun, P. S. Carney, J. C. Schotland. "Strong tip effects in near-field scanning optical tomography". *J. Appl. Phys.* 2007. 102(10): 103103.
37. B. Hecht, H. Bielefeldt, Y. Inouye, D. W. Pohl, L. Novotny. "Facts and artifacts in near-field optical microscopy". *J. Appl. Phys.* 1997. 81(6): 2492.
38. J. Kim, K.-B. Song. "Recent progress of nano-technology with SNOM". *Micron* 2007. 38(4): 409-426.
39. M. Celebrano, P. Biagioni, M. Zavelani-Rossi, D. Polli, M. Labardi, M. Allegrini, M. Finazzi, L. Duò, G. Cerullo. "Hollow-pyramid based scanning near-field optical microscope coupled to femtosecond pulses: a tool for nonlinear optics at the nanoscale". *Rev. Sci. Instrum.* 2009. 80(3): 033704.
40. J. Laverdant, S. Buil, X. Quélin. "Local field enhancements on gold and silver nanostructures for aperture near-field spectroscopy". *J. Lumin.* 2007. 127(1): 176-180.
41. T. H. Taminiou, R. J. Moerland, F. B. Segerink, L. Kuipers, N. F. van Hulst. " $\lambda/4$ resonance of an optical monopole antenna probed by single molecule fluorescence". *Nano Lett.* 2007. 7(1): 28-33.
42. K. Imura, T. Nagahara, H. Okamoto. "Near-field two-photon-induced photoluminescence from single gold nanorods and imaging of plasmon modes". *J. Phys. Chem. B* 2005. 2005(27): 13214-13220.
43. K. Imura, K. Ueno, H. Misawa, H. Okamoto. "Optical field imaging of elongated rectangular nanovoids in gold thin film". *J. Phys. Chem. C* 2013. 117(6): 2449-2454.

44. S. Kim, K. Imura, S. Kim, H. Okamoto. "Confined optical fields in nanovoid chain structures directly visualized by near-field optical imaging". *J. Phys. Chem. C* 2011. 115(5): 1548-1555.
45. M. Zavelani-Rossi, M. Celebrano, P. Biagioni, D. Polli, M. Finazzi, L. Duò, G. Cerullo, M. Labardi, M. Allegrini, J. Grand, P.-M. Adam. "Near-field second-harmonic generation in single gold nanoparticles". *Appl. Phys. Lett.* 2008. 92(9): 093119.
46. L. Duò, P. Biagioni, M. Finazzi. "Recent developments in linear and nonlinear near-field microscopy on single plasmonic nanoparticles". *Phys. Status Solidi B* 2010. 247(8): 2040-2046.
47. M. R. Shcherbakov, B. B. Tsema, A. A. Ezhov, V. I. Panov, A. A. Fedyanin. "Near-field optical polarimetry of plasmonic nanowires". *JETP Lett.* 2011. 93(93): 720-724.
48. L. Zhou, Q. Gan, F. J. Bartoli, V. Dierolf. "Direct near-field optical imaging of UV bowtie nanoantennas". *Opt. Express* 2009. 17(22): 20301-20306.
49. H.-Y. Lin, C.-H. Huang, C.-H. Chang, Y.-C. Lan, H.-C. Chui. "Direct near-field optical imaging of plasmonic resonances in metal nanoparticles pairs". *Opt. Express* 2010. 18(1): 165-172.
50. H. J. Wu, Y. Nishiyama, T. Narushima, K. Imura, H. Okamoto. "Sub-20-fs time-resolved measurements in an apertured near-field optical microscope combined with a pulse-shaping technique". *Appl. Phys. Express* 2012. 5(6): 062002.
51. A. Drezet, A. Hohenau, J. R. Krenn, M. Brun, S. Huan. "Surface plasmon mediated near-field imaging and optical addressing in nanoscience". *Micron* 2007. 38(4): 427-437.
52. J. R. Krenn, A. Dereux, J. C. Weeber, E. Bourillot, Y. Lacroute, J. P. Goudonnet, G. G. Schider, W. Gotschy, A. Leitner, F. R. Aussenegg, C. Girard. "Squeezing the optical near-field zone by plasmon coupling of metallic nanoparticles". *Phys. Rev. Lett.* 1999. 82(12): 2590-2593.
53. K. Seal, M. A. Nelson, Z. C. Ying, D. A. Genov, A. K. Sarychev, V. M. Shalae. "Growth, morphology, optical and electrical properties of semicontinuous metallic films". *Phys. Rev. B* 2003. 67(3): 035318.
54. D. Denkova, N. Verellen, A. V. Silhanek, V. K. Valev, P. Van Dorpe, V. V. Moshchalkov. "Mapping magnetic near-field distributions of plasmonic nanoantennas". *ACS Nano* 2013. 7(4): 3168-3176.
55. S. Patané, P. G. Gucciardi, M. Labardi, M. Allegrini. "Apertureless near-field optical microscopy". *Riv. Nuovo Cimento* 2004. 27(1): 1-46.
56. W. Chen, A. Kirilyuk, A. Kimel, T. Rasing. "Direct mapping of plasmonic coupling between a triangular gold island pair". *Appl. Phys. Lett.* 2012. 100(16): 163111.
57. A. Bek, R. Volgelgesang, K. Kern. "Apertureless scanning near-field optical microscope with sub 10 nm resolution". *Rev. Sci. Instrum.* 2006. 77(4): 043703.
58. A. E. Greife, D. Leiva, S. Mastel, S. D. Dhuey, S. Cabrini, P. J. Schuck, Y. Abate. "Near-field spatial mapping of strongly interacting multiple plasmonic infrared antennas". *Phys. Chem. Chem. Phys.* 2013. 15(43): 18944-18950.
59. A. Apuzzo, M. Février, R. Salas-Montiel, A. Bruyant, A. Chelnokov, G. Léronnel, B. Dagens, S. Blaize. "Observation of near-field dipolar interactions involved in a metal nanoparticle chain waveguide". *Nano Lett.* 2013. 13(3): 1000-1006.
60. M. Schnell, A. Garcia-Etxarri, A. J. Huber, K. B. Crozier, A. Borisov, J. Aizpurua, R. Hillenbrand. "Amplitude- and phase-resolved near-field mapping of infrared antenna modes by transmission-mode scattering-type near-field microscopy". *J. Phys. Chem. C* 2010. 114(16): 7341-7345.
61. F. De Angelis, G. Das, P. Candeloro, M. Patrini, M. Galli, A. Bek, M. Lazzarino, I. Maksymov, C. Liberale, L. C. Andreani, E. Di Fabrizio. "Nanoscale chemical mapping using three-dimensional adiabatic compression of surface plasmon polaritons". *Nat. Nanotechnol.* 2010. 5(1): 67-72.
62. L. Aigouy, M. Mortier, J. Giérak, E. Bourhis, Y. De Wilde, P. Corstjens, H. J. Tanke. "Field distribution on metallic and dielectric nanoparticles observed with a fluorescent near-field optical probe". *J. Appl. Phys.* 2005. 97(10): 104322.

63. A. Cuche, B. Masenelli, G. Ledoux, D. Amans, C. Dujardin, Y. Sonnefraud. "Fluorescent oxide nanoparticles adapted to active tips for near-field optics". *Nanotechnology* 2009. 20(1): 015603.
64. V. Krachmalnicoff, d. Cao, A. Caz, E. Castani, R. Pierrat, S. Collin. "Towards a full characterization of a plasmonic nanostructure with a fluorescent near-field probe". *Opt. Express* 2013. 21(9): 11536-11545.
65. Y. Sonnefraud, N. Chevalier, J.-F. Motte, S. Huant, P. Reiss, J. Bleuse. "Near-field optical imaging with a CdSe single nanocrystal-based active tip". *Opt. Express* 2006. 14(22): 10596-10602.
66. D. Sadiq, J. Shirdel, J. S. Lee, E. Selishcheva, N. Park, C. Lienau. "Adiabatic nanofocussing scattering-type optical nanoscopy of individual gold nanoparticles ". *Nano Lett.* 2011. 11(4): 1609-1613.
67. M. Breit, S. Malkmus, J. Feldmann, H. U. Danzebrink. "Near-field second harmonic generation by using uncoated silicon tips". *Appl. Phys. Lett.* 2007. 90(9): 093114.
68. R. Hillenbrand, F. Keilmann, P. Harnap, D. S. Sutherland, Aizpurua. "Coherent imaging of nanoscale plasmon patterns with a carbon nanotube probe". *Appl. Phys. Lett.* 2003. 83(2): 368.
69. P. G. Gucciardi, G. Bachelier, M. Allegrini. "Far-field background suppression in tip-modulated apertureless near-field optical microscopy". *J. Appl. Phys.* 2006. 99(9): 124309.
70. G. Longo, M. Girasole, G. Pompeo, A. Cricenti. "Optical super resolution using higher harmonics and different acquisition modes in an aperture tapping SNOM". *Phys. Status Solidi B* 2010. 247(8): 2056-2060.
71. N. Maghelli, M. Lebaridi, S. Patanè, F. Irrera, M. Allegrini. "Optical near-field harmonic demodulation in apertureless microscopy". *J. Microsc.* 2001. 202(1): 84-93.
72. R. Hillenbrand, B. Knoll, F. Keilmann. "Pure optical contrast in scattering-type scanning near-field microscopy". *J. Microsc.* 2001. 202(1): 77-83.
73. F. Keilmann, R. Hillenbrand. "Near-field microscopy by elastic light scattering from a tip". *Philos. Trans. A. Math. Phys. Eng. Sci.* 2004. 362(1817): 787-805.
74. D. C. Kohlgraf-Owens, S. Sukhov, A. Dogariu. "Optical-force-induced artifacts in scanning probe microscopy". *Opt. Lett.* 2011. 36(24): 4758-4760.
75. S. Aubert, A. Bruyant, S. Blaize, R. Bachelot, G. Lerondel, S. Hudlet, P. Royer. "Analysis of the interferometric effect of the background light in apertureless scanning near-field optical microscopy". *J. Opt. Soc. Am. B* 2003. 20(10): 2117-2124.
76. R. Esteban, R. Vogelgesang, K. Kern. "Apertureless near-field optical microscopy: differences between heterodyne interferometric and non-interferometric images.". *Ultramicroscopy* 2011. 111(9): 1469-1474.
77. L. Gomez, R. Bachelot, A. Bouhelier, G. P. Wiederrecht, S. Chang, S. K. Gray, F. Hua, S. Jeon, J. A. Rogers, M. E. Castro, S. Blaize, I. Stefanon, G. Lerondel, P. Royer. "Apertureless scanning near-field optical microscopy: a comparison between homodyne and heterodyne approaches". *J. Opt. Soc. Am. B* 2006. 23(5): 823-833.
78. M. Esslinger, J. Dorfmüller, W. Khunsin, R. Vogelgesang, K. Kern. "Background-free imaging of plasmonic structures with cross-polarized apertureless scanning near-field optical microscopy". *Rev. Sci. Instrum.* 2012. 83(3): 033704.
79. F. J. García de Abajo. "Optical excitations in electron microscopy". *Rev. Mod. Phys.* 2010. 82(1): 209-275.
80. R. Gomez-Medina, N. Yamamoto, M. Nakano, F. J. García de Abajo. "Mapping plasmons in nanoantennas via cathodoluminescence". *New J. Phys.* 2008. 10(10): 105009.
81. M. W. Knight, L. Liu, Y. Wang, L. Brown, S. Mukherjee, N. S. King, H. O. Everitt, P. Nordlander, N. J. Halas. "Aluminum plasmonic nanoantennas". *Nano Lett.* 2012. 12(11): 6000-6004.
82. E. S. Barnard, T. Coenen, E. J. R. Vesseur, A. Polman, M. L. Brongersma. "Imaging the hidden modes of ultrathin plasmonic strip antennas by cathodoluminescence". *Nano Lett.* 2011. 11(10): 4265-4269.

83. P. Chaturvedi, K. H. Hsu, A. Kumar, K. H. Fung, J. C. Mabon, N. X. Fang. "Imaging of plasmonic modes of silver nanoparticles using high-resolution cathodoluminescence spectroscopy". *ACS Nano* 2009. 3(10): 2965-2974.
84. N. J. Halas, S. Lal, W.-S. Chang, S. Link, P. Nordlander. "Plasmons in strongly coupled metallic nanostructures". *Chem. Rev.* 2011. 111(6): 3913-3961.
85. N. Yamamoto, K. Araya, F. J. García de Abajo. "Photon emission from silver particles induced by a high-energy electron beam". *Phys. Rev. B* 2001. 64(20): 205419.
86. N. Yamamoto, K. Araya, A. Toda, H. Sugiyama. "Light emission from surfaces thin films and particles induced by high-energy electron beam". *Surf. Interface Anal.* 2001. 31(2): 79-86.
87. L. Reimer, *Energy-filtering transmission electron microscopy* (Springer, Berlin, Germany, 1995).
88. D. Rossouw, M. Couillard, J. Vickery, E. Kumacheva, G. A. Botton. "Multipolar plasmonic resonances in silver nanowire antennas". *Nano Lett.* 2011. 11(4): 1499-1504.
89. D. Rossouw, G. A. Botton. "Plasmonic response of bent silver nanowires for nanophotonic subwavelength waveguiding". *Phys. Rev. Lett.* 2013. 110(6): 066801.
90. A. L. Koh, K. Bao, I. Khan, W. E. Smith, G. Kothletner, P. Nordlander, S. A. Maier, D. W. McComb. "Electron energy-loss spectroscopy silver nanoparticles and dimers: influence of beam damage and mapping of dark modes". *ACS Nano* 2009. 3(10): 3015-3022.
91. R. F. Egerton. "Limits to the spatial, energy and momentum resolution of electron energy-loss spectroscopy". *Ultramicroscopy* 2007. 107(8): 575-586.
92. A. L. Koh, A. I. Fernandez-Domínguez, D. W. McComb, S. A. Maier, J. K. W. Yang. "High-resolution mapping of electron-beam-excited plasmon modes in lithographically defined gold nanostructures". *Nano Lett.* 2011. 11(3): 1323-1330.
93. F. J. García de Abajo, M. Kociak. "Probing the photonic local density of states with electron energy loss spectroscopy". *Phys. Rev. Lett.* 2008. 100(10): 106804.
94. U. Hohenester, H. Ditlbacher, J. Krenn. "Electron-energy loss spectra of plasmonic nanoparticles". *Phys. Rev. Lett.* 2009. 103(10): 106801.
95. A. Yurtsever, R. M. van der Veen, A. H. Zewail. "Subparticle ultrafast spectrum imaging in 4D electron microscopy". *Science* 2012. 335(6064): 59-64.
96. P. E. Batson. "Plasmonic modes revealed". *Science* 2012. 335(6064): 47-48.
97. B. Barwick, D. J. Flannigan, A. H. Zewail. "Photon-induced near-field electron microscopy". *Nature* 2013. 462(7275): 902-906.
98. A. Yurtsever, A. H. Zewail. "Direct visualization of near-fields in nanoplasmonics and nanophotonics". *Nano Lett.* 2012. 12(6): 3334-3338.
99. C. Awada, G. Barbillon, F. Charra, L. Douillard, J. Greffet. "Experimental study of hot spots in gold/glass nanocomposite films by photoemission spectroscopy". *Phys. Rev. B* 2012. 85(4): 045438.
100. C. Awada, T. Popescu, L. Douillard, F. Charra, A. Perron, H. Yockell-Lelièvre, A.-L. Baudrion, P.-M. Adam, R. Bachelot. "Selective excitation of plasmon resonances of single Au Triangles by polarization-dependent light excitation". *J. Phys. Chem. C* 2012. 116(27): 14591-14598.
101. L. Douillard, F. Charra, Z. Korczak, R. Bachelot, S. Kostcheev, G. Lerondel, P.-M. Adam, P. Royer. "Short range plasmon resonators probed by photoemission electron microscopy". *Nano Lett.* 2008. 8(3): 935-940.
102. C. Hrelescu, T. K. Sau, A. L. Rogach, F. Jackel, G. Laurent, L. Douillard, F. Charra. "Selective excitation of individual plasmonic hotspots at the tips of single gold nanostars". *Nano Lett.* 2011. 11(2): 402-407.
103. R. C. Word, J. P. S. Fitzgerald, R. Könenkamp. "Direct coupling of photonic modes and surface plasmon polaritons observed in 2-photon PEEM". *Opt. Express* 2013. 21(25): 30507-30520.
104. A. Kubo, K. Onda, H. Petek, Z. Sun, Y. S. Jung, H. K. Kim. "Femtosecond imaging of surface plasmon dynamics in a nanostructured silver film". *Nano Lett.* 2005. 5(6): 1123-1127.

105. P. Melchior, D. Bayer, C. Schneider, A. Fischer, N. Rohmer, W. Pfeiffer, M. Aeschlimann. "Optical near-field interference in the excitation of a bowtie nanoantenna". *Phys. Rev. B* 2011. 83(23): 235407.
106. A. Salomon, M. Zielinski, R. Kolkowski, J. Zyss, Y. Prior. "Size and shape resonances in second harmonic generation from silver nanocavities". *J. Phys. Chem. C* 2013. 117(43): 22377-22382.
107. J. Berthelot, G. Bachelier, M. Song, P. Rai, G. Colas des Francs, A. Dereux, A. Bouhelier. "Silencing and enhancement of second-harmonic generation in optical gap antennas". *Opt. Express* 2012. 20(10): 10498-10508.
108. V. K. Valev. "Characterization of nanostructured plasmonic surfaces with second harmonic generation". *Langmuir* 2012. 28(44): 15454-15471.
109. V. K. Valev, A. V. Silhanek, Y. Jeyaram, D. Denkova, B. D. Clerq, V. Petkov, X. Zheng, V. Volskiy, G. A. E. V. W. Gillijns, A. A.O., M. Ameloot, V. V. Moshchalkov, T. Verbiest. "Hotspot decorations map plasmonic patterns with the resolution of scanning probe techniques". *Phys. Rev. Lett.* 2011. 106(22): 226803.
110. V. K. Valev, J. J. Baumberg, C. Sibita, T. Verbiest. "Chirality and chiroptical effects in plasmonic nanostructures: fundamentals, recent progress, and outlook". *Adv. Mater.* 2013. 25(18): 2517-2534.
111. T. Wang, D. Halaney, D. Ho, M. Feldman, T. E. Milner. "Two-photon luminescence properties of gold nanorods". *Biomed. Opt. Express* 2013. 4(4): 584-595.
112. A. McLeod, A. Weber-Bargioni, Z. Zhang, S. Dhuey, B. Harteneck, J. B. Neaton, S. Cabrini, P. J. Schuck. "Nonperturbative visualization of nanoscale plasmonic field distributions via photon localization microscopy". *Phys. Rev. Lett.* 2011. 106(3): 037402.
113. S. Viarbitskaya, A. Teulle, R. Marty, J. Sharma, C. Girard, A. Arbouet, E. Dujardin. "Tailoring and imaging the plasmonic local density of states in crystalline nanoprisms". *Nat. Mater.* 2013. 12(5): 426-432.
114. T. Deckert-Gaudig, V. Deckert. "Ultraflat transparent gold nanoplates ideal substrates for tip-enhanced Raman scattering experiments". *Small* 2009. 5(4): 432-436.
115. F. Pashaee, R. Hou, P. Gobbo, M. S. Workentin, F. Lagugné-Labarthe. "Tip-enhanced Raman spectroscopy of self-assembled thiolated monolayers on flat gold nanoplates using Gaussian-transverse and radially polarized excitations". *J. Phys. Chem. C* 2013. 117(30): 15639-15646.
116. T. Jägeler-Hoheisel, J. Cordeiro, O. Lecarme, A. Cucho, C. Girard, E. Dujardin, D. Peyrade, A. Arbouet. "Plasmonic shaping in gold nanoparticle three dimensional assemblies". *J. Phys. Chem. C* 2013. 117(44): 23126-23132.
117. J. A. Dionne. "Nanoplasmonics: Plasmons rock in metal bands". *Nat. Mater.* 2013. 12(5): 380-381.
118. V. K. Valev, D. Denkova, X. Zheng, A. I. Kuznetsov, C. Reinhardt, B. N. Chichkov, G. Tsutsumanova, E. J. Osley, V. Petkov, B. D. Clerq, A. V. Silhanek, Y. Jeyaram, V. Volskiy, P. A. Warburton, G. A. E. Vandenbosch, S. Russev, O. A. Atsipetrov, M. Ameloot, V. V. Moshchalkov, T. Verbiest. "Plasmon-enhanced sub-wavelength laser ablation: Plasmonic nanojets". *Adv. Mater.* 2012. 24(10): 29-35.
119. S. Dickreuter, J. Gleixner, A. Kolloch, J. Boneberg, E. Scheer, P. Leiderer. "Mapping of plasmonic resonances in nanotriangles". *Beilstein J. Nanotechnol.* 2013. 4: 588-602.
120. C. Deeb, R. Bachelot, J. Plain, A.-L. Baudrion, S. Jradi, A. Bouhelier, O. Soppera, P. K. Jain, L. Huang, C. Ecoffet, L. Balan, P. Royer. "Quantitative analysis of localized surface plasmons based on molecular probing". *ACS Nano* 2010. 4(8): 4579-4586.
121. G. Wurtz, Lougnot, R. Bachelot, F. H'Dhili, P. Royer, C. Triger, C. Ecoffet, D. J. Lougnot. "Photopolymerization induced by optical field enhancement in the vicinity of a conducting tip under laser illumination". *Jpn. J. Appl. Phys.* 2000. 39(2): 98.
122. K. Ueno, S. Takabatake, Y. Nishijima, V. Mizeikis, Y. Yokota, H. Misawa. "Nanogap-assisted surface plasmon nanolithography". *J. Phys. Chem. Lett.* 2010. 1(3): 657-662.

123. G. Volpe, M. Noack, S. Acimovic, C. Reinhardt, R. Quidant. "Near-field mapping of plasmonic antennas by multiphoton absorption in poly(methyl methacrylate)". *Nano Lett.* 2012. 12(9): 4864-4868.
124. Y. Gilbert, R. Bachelot, A. Vial, G. Lerondel, P. Royer, A. Bouhelier, G. P. Wiederrecht. "Photoresponsive polymers for topographic simulation of the optical near-field of a nanometer sized gold tip in a highly focused beam". *Opt. Express* 2005. 13(10): 3619-3624.
125. B. Galarreta, I. Rugar, A. Young, F. Lagugné-Labarthe. "Mapping hot-spots in hexagonal arrays of metallic nanotriangles". *J. Phys. Chem. C* 2011. 115(31): 15318-15323.
126. C. Hubert, R. Bachelot, J. Plain, S. Kostcheev, G. Lerondel, M. Juan, P. Royer, S. Zou, G. C. Schatz, G. P. Wiederrecht. "Near-field polarization effects in molecular-motion-induced photochemical imaging". *J. Phys. Chem. C* 2008. 112(11): 4111-4116.
127. M. L. Juan, J. Plain, R. Bachelot, P. Royer, S. K. Gray, G. P. Wiederrecht. "Multiscale model for photoinduced molecular motion in azo polymers". *ACS Nano* 2009. 3(6): 1573-1579.
128. M. Tabatabaei, A. Sangar, N. Kazemi-Zanjani, P. Torchio, A. Merlen, F. Lagugné-Labarthe. "Optical properties of silver and gold tetrahedral nanopyramid arrays prepared by nanosphere lithography". *J. Phys. Chem. C* 2013. 117(28): 14778-14786.
129. T. Koenig, L. M. Goldenberg, O. Kulikovska, L. Kulikovsky, J. Stumpe, S. Santer. "Reversible structuring of photosensitive polymer films by surface plasmon near field radiation". *Soft Matter* 2011. 7(9): 4174-4178.
130. D. Dregely, F. Neubrech, H. Duan, R. Vogelgesang, H. Giessen. "Vibrational near-field mapping of planar and buried three-dimensional plasmonic nanostructures". *Nat. Commun.* 2013. 4: 2337.
131. K. Gibson, D. Correia-Ledo, M. Couture, D. Graham, J. F. Masson. "Correlated AFM and SERS imaging of the transition from nanotriangle to nanohole arrays". *Chem. Commun.* 2011. 47(12): 3404-3406.
132. J. Kohoutek, D. Dey, A. Bonakdar, R. Gelfand, A. Sklar, O. G. Memis, H. Mohseni. "Opto-mechanical force mapping of deep subwavelength plasmonic modes". *Nano Lett.* 2011. 11(8): 3378-3382.